Microplastics in farmlands: A model of conditional fragmentation and source estimation

Dong Sheng[1,2,3]*, Feng Ju[4], Ling Li[2†], Thomas Cherico Wanger[3,5*†]

1. College of Environmental and Resource Sciences, Zhejiang University, Hangzhou 310058, China
2. Key Laboratory of Coastal Environment and Resources of Zhejiang Province, School of Engineering, Westlake University, Hangzhou 310030, China
3. Production Technology and Diversified Cropping Systems Group, Agroscope, Nyon 1260, Switzerland
4. Environmental Microbiome and Biotechnology Laboratory, Center of Synthetic Biology and Integrated Bioengineering, School of Engineering, Westlake University, Hangzhou 310030, China
5. Academy of Global Food Economics and Policy, China Agricultural University, Beijing 100083, China

* Correspondence: DS(shengdong@westlake.edu.cn), TCW(tomcwanger@gmail.com)
† These authors jointly supervised this work

Abstract: Microplastic (MP) pollution in agricultural systems has emerged as a critical environmental concern, yet quantitative models capturing the complex dynamics of MP fragmentation and accumulation remain underdeveloped. Here we present a cross-scale modeling framework that solves fragmentation mechanisms and input sources at the same time, and simulates the temporal evolution of MP size distributions in agricultural soils. The model captures the size-dependency of MP fragmentation rates and estimates the input intensity of different pollution sources. We synthesized literature data from 98 studies, covering 438 agricultural sites and 3235 datapoints across 16 countries. Parameter optimization using Huber loss (robust R^2 = 0.412) showed higher performance than regression-based approaches, and showed that fragmentation rates are dependent on particle sizes, and influenced by climate types and cropping cycles. In general, MP fragmentation rates decrease as they break into smaller sizes. Comparing different site conditions, large MP particles (> 40 μm) experience faster fragmentation under high-UV climates due to more intense photoaging, which is further accelerated by mechanical disturbance depending on cropping cycles. On the other hand, small MP particles (< 40 μm) break down faster under low-UV climates, likely due to biological aging from soil microbes and hydrological cyclic micro-stress. Of the long-term MP input sources including mulch films, plastic greenhouses, organic fertilizers, wastewater irrigation, atmospheric deposition, and unmanaged littering, plastic mulch films were the primary contributor to the mass of soil MPs (around 5.8 mg/kg after 5 years) across all climate types and cropping cycles. If measured by particle abundance, organic fertilization introduces the highest MP abundance in soil at the first 5 years (1.1×10^3 items/kg) as they contain numerous small-sized MPs. A case study on China's mulching history showed strong regional heterogeneity in MP accumulation, with legacy plastics continuing to generate secondary MPs even under zero-new-input scenarios. This work provides a theoretically grounded and empirically calibrated tool for assessing MP pollution dynamics and management strategies in agricultural systems from local to global scale.

Keywords: microplastics, fragmentation, agriculture soils, modelling, input sources

Introduction

Global plastic use in agricultural production has reached 7.4 million tons and been steeply increasing by 2.5 million tons annually.[1] Consequently, microplastic (MP) pollution in terrestrial ecosystems, and in agricultural soils particularly, has emerged as a critical concern to the environment and food security.[2,3] Soils act as the primary receptor for MP emissions and subsequently expose many species to plastic pollution including plants, soil microbiome, insects, and other biota.[4] Currently a structured quantification of the transformations and fate of MP in agricultural soils is missing but urgently needed.

Quantification of soil microplastic pollution needs to integrate multiple input sources that determine the initial size and downstream susceptibility to complex transformation processes. First, multiple sources contribute to MP entering agricultural soils (Figure 1a) such as plastic mulch films, atmospheric deposition, wastewater irrigation, organic fertilizers (compost, sewage sludge, etc.), and littering.[5,6] These sources exhibit various distinct characteristics. For instance, MPs from atmospheric deposition and organic fertilizers tend to have a large proportion of small-sized particles,[7,8] whereas mulching residuals enter the soils as large pieces of films. Second, MPs in the soil experience complex aging and fragmentation processes (Figure 1b). Photoaging induced by ultraviolet (UV) irradiation leads to increased reactive oxygen species (ROS), surface roughness,[9] and fragmentation.[10] Certain microbes also cause biotic aging with increased hydrophilicity[11] and surface roughness.[12–14] Noticeably, biotic aging efficiency is largely influenced by prior photoaging processes.[15] Fragmentation can be caused by various external forces. Agricultural practices such as tillage exerts a macro-scale mechanical disturbance on MPs, which varies by cropping cycles (annual vs perennial). Moreover, the wetting and drying process of agricultural soil creates a cyclic micro-scale stress across soil aggregates that may lead to MP fragmentation.[16,17]

Ultimately, MP particle size is a critical factor on the relative intensity of aging and fragmentation drivers. For instance, small MPs may experience faster biotic aging due to increased specific surface area.[12,18] The aggregation of MPs and soil granules is also dependent on particle size, as small MPs are more likely to be incorporated into soil aggregates[19–21] through van der Waals forces, electrostatic attractions,[22] and binding with extracellular polymeric substances.[20] Therefore, MP pollution in agricultural soils represents a complex, size-dependent system governed by the interplay between diverse input sources and in-situ transformation mechanisms. The nonlinear temporal evolution of these processes makes it exceptionally challenging to isolate the standalone effects of specific drivers through field observations, as environmental samples invariably reflect a cumulative history of multiple overlapping factors. Therefore, environmental modeling emerges as a critical tool to reconstruct these pathways and identify the dominant causes shaping MP distributions observed in field samples. While several models have been

developed to describe MP fragmentation in terrestrial/marine ecosystems, they exhibit critical limitations when applied to agricultural soils (
Table 1). Some early marine-based models introduced important mechanisms such as pre-determined size thresholds[23] or combined with shear forces,[24] but their applicability to terrestrial systems is limited. A more physically grounded approach was taken by Kaandorp et al. to simulate erosion into multiple child particles at diverse sizes in marine environments, but lacked size-dependency.[25] Other models with a focus on the soil context have addressed specific aspects: Meizoso-Regueira et al. forecasted the nonlinear abundance growth via statistical regression;[26] Quik et al. developed a multimedia model to include soil, but ignored size-dependency;[27] Wang et al. proposed a size-dependent model for MP in soils, but omitted temporal evolution.[28]

Here we propose a cross-scale modelling framework designed to represent complex environmental systems where multiple mechanisms contribute to a same process. We used the universal variable "MP fragmentation rate" to represent the sum of all effects (Figure 1c), which simplifies the model structure and avoids the need of numerous poorly constrained mechanisms. It also allows for incorporating heterogeneous observational data at different size ranges. Our model integrates two major extensions into the cascading fragmentation theory:[25] size-dependent fragmentation dynamics and multiple input sources with unique initial size distributions. The framework enables a temporally resolved reconstruction of MP fragmentation and accumulation in agricultural soils, which can support real-world applications. As a case study, we apply the model to China, where the widespread use of plastic mulch films (> 2.5 million tons annually)[29] has created one of the largest known sources of agricultural plastic pollution.[1] We combined historical mulching data with literature-derived model parameters, and projected mulching-derived MP pollution under different policy scenarios. With the proposed model framework, this study aims to: (i) optimize model parameters using literature data and (ii) address the following research questions:

- Is size-dependent fragmentation empirically supported in agricultural soils?
- How do environmental factors and crop types influence fragmentation rates?
- What are the dominant input sources for MP pollution in agricultural soils?
- Using the historical mulching data in China as a case study, what are the projected long-term trends of MP pollution in agricultural soils under different policy scenarios?

Results

Model optimization results

The optimized model's performance was evaluated on the complete dataset of 438 agricultural sites (3235 datapoints) and validated on a subset of long-term field data (5 studies), with comparison to the performance of a regression-based benchmark model

(Table S1). Intuitively, the predictions of our model are generally aligned with the distribution of observational data, with some exceptions at the upper and lower extremes (Figure S1a). We reached a robust R^2 (defined on Huber loss) of 0.412 on the complete dataset, which indicates that the model captured the general trends in MP pollution. The median absolute error of model predictions was 200.49 items/kg, which is one magnitude smaller than to the main body of the dataset (>10^3 items/kg; Figure 2a). The modest prediction coverage (43.18%) reflects the highly dispersed field data and a relatively simple model that narrows the span of predicted distributions. Noticeably, validation on time-series literature data yielded a higher robust R^2 (0.586) and prediction coverage (90.48%). This demonstrates the model's ability to effectively predict the temporal dynamics of MP accumulation in a given agricultural site over the span of decades (Figure 2b). Our model out-performed the benchmark across all the metrics (Table S1 and Figure S1), showing the advantages of the process-based approach over simple and commonly used regression methods.

Factors affecting fragmentation rates

MP fragmentation rates are size-dependent across climate conditions and cropping cycles. Large MPs experience stronger fragmentation compared to small MPs ($p < 0.001$; Figure 3a), and a shifting point was optimized at around 40 μm (median θ = 7.05, β = 3.81). For small MPs, the median fragmentation rate was 1.00×10^{-6} week^{-1} ($Q_1 = 4.49 \times 10^{-7}$, $Q_3 = 1.34 \times 10^{-6}$) in low UV climates and 1.23×10^{-10} week^{-1} ($Q_1 = 9.28 \times 10^{-11}$, $Q_3 = 2.23 \times 10^{-10}$) in high UV climates (Figure 3b), indicating mild and humid climates facilitates fragmentation of small MPs ($p < 0.001$) possibly through an active soil microbiota and frequent wet-dry cycles. For large MPs, the fragmentation rate reached 1.15×10^{-5} week^{-1} ($Q_1 = 8.29 \times 10^{-6}$, $Q_3 = 1.61 \times 10^{-5}$) in low UV climates and 5.81×10^{-4} week^{-1} ($Q_1 = 5.04 \times 10^{-4}$, $Q_3 = 9.03 \times 10^{-4}$) in high UV ones (Figure 3b-d), showing enhanced fragmentation with photoaging at larger size classes ($p < 0.001$). Annual cropping increased MP fragmentation by 6.85×10^{-5} week^{-1} ($Q_1 = 5.57 \times 10^{-5}$, $Q_3 = 9.97 \times 10^{-5}$) relative to perennial systems, reflecting the influence of macro-level mechanical disturbance ($p < 0.001$). For detailed results of optimized parameters, see Table S2.

Long-term impact of input sources

To evaluate the long-term input intensity across different sources, we simulated the MP accumulation under contrasting cropping systems and climate types after 5, 25, and 75 years of continuous input. The influence of different input sources varies depending on the local climate types, cropping cycles and measuring metrics (mass or abundance). For annual crop sites under high-UV climate conditions (Table S3), plastic mulching contributed the largest mass accumulation throughout the years (Figure 4). However, if measured by particle abundance, organic fertilizer is ranked as the primary source of MP within the first several decades. Plastic mulching becomes increasingly prominent and reached the highest abundance on the long run (Figure 4b). The different growing patterns in abundance is explained by size distributions (Figure 4c), where sources with more large MPs grows faster in abundance as MPs fragment into smaller ones (Figure 3a). Under low-UV climates (Figure S2; Table S4), MPs in soil show similar mass accumulation but different abundance and size distribution patterns due to altered fragmentation rates. The results for perennial cropping systems are presented in Figure S3–4 and Table S5–6. Soils in these sites receive lower MP inputs from atmospheric deposition as a result of denser canopy cover, and experience reduced fragmentation for large MPs because of less mechanical disturbance.

Theoretical single-particle evolution

We simulated the evolution of a single parent MP particle under different climate types and cropping cycles. Under high UV, the size distribution developed a temporal peak at an intermediate size (around 40 μm), which then starts to decrease after 500 years (Figure 5a). For low-UV climates, the peak is weaker and more MPs appear at the small sizes (Figure 5b). Perennial sites showed slower fragmentation and retained a higher proportion of larger particles (Figure S5). These temporal contrasting patterns originate from the conditional size-dependent fragmentation rates.

Model sensitivity

We performed a local sensitivity analysis to test model's response towards parameter perturbations. The model is considered robust against the parameter perturbations at 5% and 10% level as the response of the loss values are consistently smaller than the level of parameter disturbance (Figure 6).

Our data imputation on missing planting histories and lower bounds of particle size did not bring substantial changes to the results of fragmentation rate parameters, but roughly doubled the input intensity of greenhouses, littering and organic fertilizers (Table S7), which shows uncertainties on estimating emissions due to missing data. However, these changes did not threaten our major findings as the conditional fragmentation patterns and the relative importance of different input sources remained steady.

Case study: decades of mulching in China

The provincial-level simulations revealed strong regional heterogeneity in mulching-derived MP accumulation across China (Figure 7). Provinces with historically intensive mulching practices show substantially higher MP concentrations across all scenarios. Under the Business-as-Usual scenario, large MP particles (> 1767.8 μm) continue to accumulate in several major agricultural regions by 2050. Reducing mulch-film residues in croplands can lower the projected abundance of large MPs, demonstrating the effectiveness of controlling future plastic inputs. As existing MPs continues to fragment into substantial amounts of secondary smaller MPs even under the No-Mulching-Residuals scenario, legacy plastic residues will remain an important long-term source of MP pollution even if new inputs could be eliminated. The size distribution of MPs also differs systematically across climatic regions. In high-UV provinces, fragmentation processes promote the accumulation of middle-sized particles, (55.2–1767.8 μm), while low-UV provinces exhibit stronger accumulation of smaller particles due to faster fragmentation on fine MPs (6.9–55.2 μm). These results suggest that future environmental risks may differ regionally with croplands under high-UV climates facing greater exposure to large- and middle-sized MPs, whereas croplands in low-UV regions feature finer MP particles.

Discussion

In this study, we introduced a modelling framework that describes MP transformation in terrestrial systems. Instead of explicitly assigning each mechanism with poorly constrained parameters, we addressed this challenge by aggregating all fragmentation mechanisms into a general parameter that implicitly captures the combined effects within each size range. This approach simplifies model structure while retaining the ability to reproduce MP size distributions in good coherence with time-series observations.[30–32] It enabled us to use data from very broad experimental settings for parameter estimation. We proposed a practical approach to integrate the fragmented literature evidences into a coherent modelling framework for complex environmental systems.

Our results show that MP fragmentation in agricultural soils is size-dependent with large MPs fragmenting much faster than smaller ones. We found local climate conditions (UV radiation) and cropping cycles as effective indicators of fragmentation patterns. High-UV climates facilitate the break-down of large MPs, whereas low-UV climates accelerate the rates of small MPs. Cropping cycles also play a crucial role, particularly for large MPs. This indicates that large particles are mainly driven by UV-driven photoaging and mechanical disturbance from tillage, whereas smaller particles are more likely to be influenced by interactions with soil microbiota and soil aggregates. We found similar patterns in MP fragmentation rates with previous works. For instance, Wang et al.[28] reported accelerated MP downsizing with agricultural interference, which is aligned with our findings that annual cropping speeds up MP fragmentation. For large MPs in agricultural soils, our estimations were about 2 magnitudes lower than the estimations of modelling work from marine environments,[25] which is expected because the latter should reproduce MP fragmentation in marine sandy beaches with high UV exposure and mechanical abrasion disturbance.[10] For small MP particles, our results on fragmentation rates under low-UV climates were similar to previous estimates of biological aging rates.[27]

As MP accumulation and fragmentation in the soils is a dynamic process, we found the contributions of different MP sources to vary depending on site conditions, metrics of measurement, and the years of practice. Although the use of mulch films is the major source of MPs in terms of total mass, other indirect input sources such as organic fertilizers and wastewater irrigation also contribute substantially to soil MP pollution especially when measured by particle abundance. This is worth noticing as current understandings of agricultural plastic pollution, for instance in the reports of FAO, is mainly built around direct inputs from plastic products.[33] A more comprehensive narrative that incorporates unintentional input sources is needed to highlight the risks of agricultural plastic pollution in the ongoing negotiations of Global Plastic Treaty.

Our case study on plastic mulching in China demonstrated the practical value for environmental assessments and policy analysis of the model. Plastic mulching has expanded rapidly over the past decades in China due to its benefits for crop productivity and water conservation.[34] However, incomplete recovery of residual films has led to substantial plastic accumulation in farmland soils. We combined historical data with estimated parameters from the literature to reconstruct mulching-induced MP accumulation at multi-decadal timescales, and subsequently project future trends under alternative mulching scenarios. Such modelling tools can support the evaluation of policy interventions that target mulch residual recovery and the adoption of biodegradable films.[29]

Our model is an excellent starting point to enable broad scale quantification of the dynamics of plastic pollution in agricultural soils. However, we could not incorporate all potentially relevant factors, such as plastic types, soil properties, and local weather conditions, and our compiled dataset is relatively coarse, both due to the limitations of available literature. The available literature may also omit important information of MP input sources, for instance, organic fertilizer application or wastewater irrigation may not be clearly described for a site if it was not key variable of interest. We propose four research directions to improve future modelling efforts and the understanding of MPs in agricultural soils. i) Quantifying micro-scale mechanisms of MP fragmentation to constraint for future models; ii) Expanding detection limits of analytical techniques for plastic pollution to validate fragmentation models and better characterize the full spectrum of MP sizes in soils; More generally iii) developing remediation strategies to handle legacy MPs in agricultural soils is critical to minimize future MP impacts on agricultural landscapes and food systems; and iv) linking MPs in agricultural soils to crop production and regulating ecosystem services for an improved systems perspective of plastic pollution in agricultural landscapes (for more details see Box 1). Overall, the modelling framework may be applied to other agricultural regions with intense plastic inputs and limited long-term monitoring data. This work is critical to inform implications of plastic pollution on crop production, production related ecosystem services such as pollination and pest control as well as on food security.

Materials and methods

Data collection and process

Data preparation

We searched on Web of Science with the pattern "TS = ((nanoplastic* OR microplastic*) AND (agricultur* OR farm*) AND soil* AND (size* or length*) AND (abundance* OR concentration*))" on April 9, 2026. Literature reviews were excluded, resulting in 342 relevant publications, among which 98 papers reported MP abundance in agricultural soil along with size distribution data. In total, we extracted 438 data entries, each corresponding to either a distinct agricultural field, experimental treatment, or a group of sites with the same conditions. For each data entry, the recorded variables included MP size bins (a total of 3235 datapoints) and corresponding abundance values (items/kg), as well as site location, planting history (years), crop type (annual or perennial), and the presence of potential microplastic input sources on each site (i.e., mulching, greenhouses, organic fertilizers, wastewater irrigation, and littering; for detailed descriptions of each source, see section "*Input sources and temporal evolution"* below). Numerical variables were either acquired from the texts or measured from graphs using Web Plot Digitizer (version 4.8, https://apps.automeris.io/wpd4/).

The agricultural sites were classified according to the primary Köppen climate types (http://www.geodata.cn) of the locations, and grouped into high UV climates and low UV climates. The high-UV group includes Am (tropical monsoon), Aw (tropical savanna with dry winters), Bw (arid), Bs (semi-arid), Cs (Mediterranean) and ET. These climates are governed by strong persistent or seasonal drought, where intense UV radiation and thermal oxidation may dominate MP fragmentation. On the other hand, the low-UV group includes Cf (humid temperate), Cw (temperate with dry winters), Df (humid continental), and Dw (continental with dry winters). These climate types feature low UV radiation and high humidity throughout the years or in the growing seasons, which potentially supports active microbial communities and frequent wet-dry cycles in the soil.[35] The final dataset covers sites from a broad range of climate conditions across 16 countries (Table S8).

Apart from soil MP pollution, we also collected literature on MP size-distribution from multiple input sources, including organic fertilizers, wastewater irrigation, and atmospheric deposition. This is essential for calibrating different input sources in our model. For details, see the section *Input sources and temporal evolution* below and Table S9.

Handling ambiguous and missing data

The dataset posed challenges in data clarity and completeness. First, about 19% of the studies reported planting history imprecisely, providing only a range of possible years, or one of the upper/lower bounds. In such cases, we adopted a uniform random distribution using the reported range, or a 25% extension window applied to boundary values. For example, if a site has been cropped for "more than 10 years", we assume its planting history as a random number between 10 years and 12.5 years. For data entries with unknown planting history (which takes up 50% of our dataset), we estimated the ranges of planting history using empirical criteria (Method S1; Figure S6) based on information of input sources, and then applied uniform distribution on the inferred planting history. Second, about 63% of the data entries lack the lower limit of the smallest size class for MP distribution. Given that particle size distribution tend to follow a power-law distribution,[10] the lower bound of each size class is essential for estimating particle counts. We set the unknown lower limits as the corresponding upper limits divided by 6.22, which is the average upper limit–lower limit ratio for the smallest size classes with fixed boundaries.

Model design

Size-dependent cascading fragmentation

Kaandorp et al.[25] developed a continuous cascading fragmentation model to simulate the size distribution of MPs in the marine environment[36] based on fractal theory. MP particles are grouped into distinct size classes. The size of the k-th class is $L_k = L_0/2^k$, where L_0 is the characteristic size of the parent MP particle at class $k = 0$. Considering the size definition of MPs (1 μm – 5 mm) and data resolution, we set L_0 as 5 mm, and modelled up to 10 distinct classes (smallest class with a characteristic size of 9.76 μm). The original size classes from the literature were re-binned into the same size classes of our model, with the assumption that MP abundance within a size bin is evenly distributed across the log-transformed particle size. Following a cascading fragmentation process, the mass size distribution can be described as

$$m(k,f) = \frac{\Gamma(k+f-1)}{\Gamma(k+1)\cdot\Gamma(f)}\cdot p^k\cdot(1-p) \qquad (1)$$

where $f \in (0,+\infty)$ marks the progress of fragmentation, and $p \in (0,1)$ is the probability of fragmentation. Kaandorp et al. found the values of p to be approximately 0.4 for different plastic materials, including polyethylene (PE) and polypropylene (PP).[25] Given that most of the plastic types in our dataset (e.g., polystyrene (PS), polyvinyl chloride (PVS), PE and PP) are resistant to biodegradation with a hydrocarbon backbone, we fixed p as 0.4 for our model. The dimensionality of MP particles determines how many child particles can be created. With a given dimensionality D_N, we can then calculate the abundance size distribution as

$$n(k,f) = 2^{D_N k} \cdot m(k,f) \tag{2}$$

Based on the shape distribution of MP particles in our dataset (Method S2, Figure S7), we set the dimensionality D_N to follow a uniform random distribution between 1.4 and 2.4.

In the original model for marine environments, the fragmentation index f was assumed to be size-invariant and proportional to time (i.e., $f \equiv \lambda \cdot t$), making the fragmentation rate λ a constant. However, this is not the case within agricultural soil profiles. As large MPs fragment into smaller ones, they are more likely to be incorporated into soil aggregates,[19,22,37] which reduces the impact of UV irradiation and macro-level mechanical abrasion.[10] On the other hand, the wetting and drying process inserts a cyclic micro-stress to soil aggregates and the incorporated small MPs.[16,17] The larger specific surface area of small MPs also introduces more intense interaction with soil microbes, thus accelerating biotic aging.[12,18] To capture the size-dependent driver intensity, we define the fragmentation rate

$$\ln \lambda = \ln a + \frac{\ln b - \ln a}{1 + e^{-\beta \cdot (k-\theta)}} \tag{3}$$

where a and b are the limits of fragmentation rate for large MP and small MP respectively, θ is the threshold size, and β describes the steepness of the transition.

We assume that the fragmentation of large MPs is governed by photoaging from UV irradiation as well as mechanical disturbance from tillage (annual crops vs. perennial crops). This is considered more intense in the high UV climates of our classification. For small MPs, fragmentation is dominated by biological aging and hydrological cyclic micro-stress. In the low UV climate group, we expect a stronger biological aging effect because the soils tend to harbor more active microbial communities,[35] and weaker photoaging process can facilitate the enrichment of plastic-degrading microbes.[15] The high precipitation in such climates also accelerates wet-dry cycling, thereby intensifying the cyclic micro-stress on small MPs. We express the fragmentation limits as

$$\begin{aligned} a &= a_0 \cdot (1 - \mathrm{uv}) + a_1 \cdot \mathrm{uv} + \delta_a \cdot \mathrm{annual} \\ b &= b_0 \cdot (1 - \mathrm{uv}) + b_1 \cdot \mathrm{uv} \end{aligned} \tag{4}$$

where a_0 is the fragmentation limit in low-UV climates for large MPs, b_0 is the limit in low-UV climates for small MPs, a_1, b_1 are the limits under high-UV climates, and δ_a is the increased mechanical disturbance effect between annual cropping and perennial cropping. uv and annual are Boolean variables used to represent the respective site conditions.

Input sources and temporal evolution

In a polluted agricultural site, the size distribution of MPs in soil is not only determined by the fragmentation process, but also by multiple source emissions at the same time. In our model, the time series of MP size distribution are updated in a Markov process

$$\boldsymbol{Y}(t+\Delta t) = \boldsymbol{T} \cdot \left(\boldsymbol{Y}(t) + \sum_{i \in S} \alpha_i \cdot \mathbf{Input}_i \right) \quad (5)$$

where $\boldsymbol{Y}(t)$ is the array of MP size distribution at a given time t, $\mathbf{Input}_i$ is the input array of emission source i, and $\boldsymbol{T}$ is the transition matrix (Method S3) that controls the transition at timestep Δt (corresponds to 1 week as in the original model).[25] This model structure assumes the system is mass-conservative aside from external inputs, although MPs that fragment into sizes below our defined size classes are considered unobservable. As the influences of vertical downward transport is ~0.5% mass loss per annum in the top 8 cm soil layer,[38] and biological mineralization is less than 0.3% across size classes,[39] these factors are not considered in our model (Method S4).

Depending on farming practices and management strategies, agricultural soils are exposed to multiple MP input sources with distinct characteristics. In this work, we categorize the sources into six major types as identified in existing literature: plastic mulching, greenhouses, organic fertilizers, wastewater irrigation, atmospheric deposition, and unmanaged littering.[3,5,6] Detailed settings for each input source are as follows.

Plastic mulching is a widely applied agricultural technique to create a warmer micro-climate at the roots and increase soil moisture levels. Over one million tons of plastic films are used globally each year, with China, Japan, and South Korea being the top three consumer countries.[34] It is considered a primary source of MP pollution in agricultural systems.[40,41] Mulching MP enters the soil as large pieces of films, and generates secondary MP through in-situ fragmentation. Therefore, in our model, applications of mulching only introduce MP input at the largest size class ($k = 0$).

Greenhouse cultivation offers several advantages to crop production, such as resilience to extreme weathers and prevention of pests. The plastic films of greenhouses is another potential source of MP pollution.[42] Similar to mulching films, the leftovers of greenhouse films generate secondary MP through fragmentation. In our model, we also simplify the MP input of greenhouses as only at the largest size class.

Organic fertilizers are carbon-based materials such as compost, sewage sludge, and livestock feces, which are applied to soil to supply plant nutrients and improve soil properties as alternatives to chemical fertilizers. The incorporation of MP into organic fertilizers occurs through contaminated source materials and production process, which makes it an important source for MP to enter agricultural soils.[8] We synthesized the MP size distribution of various organic fertilizers (crop residues, livestock feces, sewage sludges, etc.) from literature data,[8,43–48] and used log-log quadratic regression (Figure S8a; Table S9) to determine the abundance-size relation that was then used as the general input size distribution of MP from organic fertilizers.

Wastewater irrigation conserves freshwater resources and at the same time introduces MP directly into agricultural soils.[49] Although wastewater treatment plants can sometimes eliminate > 90% MP,[45] the processed effluent still contain an important amount of MP. As a potential source of MP, irrigation wastewater has received much lesser attention compared to organic fertilizers. Therefore, we supplemented our literature data[49,50] with studies on the removal efficiency of wastewater treatment plants[45,51] (Figure S8b; Table S9). We then performed log-transformation and quadratic regression to capture the general size distribution of MP input from wastewater irrigation.

Atmospheric deposition is a critical pathway of MP redistribution,[52] and the deposition fluxes is affected by the land-use types and MP particle sizes.[53] We synthesized literature data on the atmospheric deposition of MP in rural or suburban areas globally,[7,53–63] and then used the same method as we did for organic fertilizers wastewater irrigation to calculate the input size distribution for our model (Figure S8c; Table S9). In perennial cropping systems, we assumed airborne MPs to be partially retained by canopy cover to one third of the original inputs. In greenhouse systems, airborne MPs were assumed to be effectively blocked. These values represent structural scenario assumptions to capture differences in interception efficiency across land-use types. Atmospheric deposition is treated as a baseline background input present in all regions.

Littering of plastic wastes such as used plastic bags and bottles, especially in poorly managed farmlands or sites near landfills, also contributes to the accumulation of MP.[64] This is simplified as input at the largest size class in our model.

Model fitting

Parameter optimization

Our model parameters, including fragmentation-related parameters and source-specific emission intensities, were estimated by minimizing the difference between predictions and observational data. To ensure robustness against extreme outliers in the skewed dataset, we used Huber loss[65] as the objective function for optimization:

$$\text{Loss} = \sum L_\delta(\hat{y} - y) \tag{6}$$

where $\hat{y}$ is the predicted MP abundance value of observational data point y. The Huber loss function L_δ is defined as:

$$L_\delta(\hat{y}-y)=\begin{cases}\frac{1}{2}(\hat{y}-y)^2, & |\hat{y}-y|<\delta \\ \delta\cdot\left(|\hat{y}-y|-\frac{1}{2}\delta\right), & |\hat{y}-y|\geq\delta\end{cases} \tag{7}$$

The function act as the mean squared error for small residuals ($|\hat{y}-y|<\delta$) and as linear loss for larger residuals ($|\hat{y}-y|\geq\delta$). We set the threshold δ to the 90th percentile of the absolute residuals from the model run, providing an adaptive criterion to changes during the optimization process.

The minimization of the loss function was conducted in a two-stage process for better efficiency. We firstly performed global search using the dual annealing algorithm[66] implemented in the SciPy package (version 1.16.3, Python 3.12). The hyperparameters were set as follows: initial temperature = 5×10^4, restart temperature ratio = 1×10^{-4}, and visiting parameter = 2.85. The parameter set with the lowest loss value from the dual annealing stage was then used as the initial guess for a subsequent local refinement using the L-BFGS-B method (a time- and memory-efficient minimization algorithm with good performance for non-smooth problems),[67] which is also implemented in SciPy. Parameters a and b were log-transformed within the optimization search space to stabilize the search process by mitigating scaling issues when values approach zero. Uncertain planting history and particle dimensions were set as the median values of the inferred uniform distribution at this primary stage. To avoid falling into local minimal basins, this process was conducted in three batches with different random seeds, and we picked the smallest loss value as the result of primary optimization.

After the primary optimization, we performed a Bag of Little Bootstraps (BLB) estimation to address uncertainties. The BLB method combines bootstrapping with subsampling, therefore enables analyzing massive datasets under limited computation resources.[68] Given that the step-wise matrix multiplications in our model have a computational complexity that increases quadratically with the number of data entries, BLB proves especially valuable under computational constraints. We generated 3000 subsamples by randomly drawing 100 data entries from the original dataset without replacement. Then for each subsample, we randomly assigned the particle dimension (see equation (2)) and planting history (see section *"Handling ambiguous and missing data"*). Afterwards, we created a bootstrap replicate from this subsample by resampling its observations with replacement, yielding a final bootstrap sample. Using the primary optimization results as initial values, we conducted the local refinement optimization on each bootstrap replicate with the L-BFGS-B algorithm. Optimization results exceeding the search space (Table S10) were removed. The resulting parameter sets were then used to generate a distribution of predictions for model evaluation and statistical analysis.

Model performance evaluation

We used the median values of model predictions for direct comparison with observational data. As a visual preliminary assessment, we plotted the histograms of observations and predictions in the log space to check the overall distributional alignment, as well as the residuals vs. predictions to examine the independence of errors. Since the dataset is skewed with a few extreme outliers, and since the model was optimized with Huber loss instead of Residual Sum of Squares (RSS), the conventional R^2 is not an accurate reflection of the fitting performance. Therefore, we constructed a robust R^2 based on the criteria of the Huber loss function:

$$R^2_{\mathrm{robust}} = 1 - \frac{L_\delta(\hat{y} - y)}{L_\delta(\overline{y} - y)} \tag{8}$$

where y is the observed value, $\hat{y}$ is the median point of prediction, and $\overline{y}$ is the average value of observations. The loss function L_δ is defined as in equation (7). When the residuals fall within the threshold δ, the metric reduces to the conventional R^2. We also reported the median absolute error (MedAE) and mean absolute error (MAE) on both original and log-transformed data, as well as Pearson correlation. Apart from using the median prediction values, we calculated the coverage on observational data from the 95% prediction interval. We further validated our model's performance by simulating with site-specific conditions from five publications that reported time-series MP accumulation of the same or similar sites.[30,32,69–71] To showcase the advantage of our process-based modelling approach over commonly used statistical methods, we adopted Meizoso-Regueira et al.'s regression-based prediction model[24] for our dataset, and used its prediction results as a benchmark for performance evaluation (details in Method S5).

Statistical analysis for fragmentation rates and sources

We performed a Kruskal-Wallis H test followed by Bonferroni-adjusted post hoc Mann-Whitney U tests to evaluate the effects of climate types (high UV vs. low UV) and cropping cycles (annual vs. perennial) on MP fragmentation rates. To assess the long-term input intensity from different sources, we simulated the accumulation of MP after 5, 25, and 75 years of continuous input (from 2025 to 2030, 2050, and 2100), and compared across sources based on total mass and particle abundance and size distribution. The mass of a particle at size class k was estimated as

$$m_k = \rho \cdot L_k^{D_N} \cdot l_{\min}^{3-D_N} \tag{9}$$

where ρ is the density (assumed as 1 g/cm^3), L_k is the characteristic size of MP in size class k, D_N is the particle dimension, and $l_{\min}$ is the lower bound of the smallest MP size class defined in our model. The same statistical method was used for comparing different sources.

Theoretical analysis of single-particle evolution

To further explore the intrinsic dynamics of the model under idealized conditions, we simulated the long-term evolution of a single parent MP particle (largest size class $k = 0$) without any subsequent external input. The system was then allowed to evolve under four settings as the combination of high/low UV irradiation and annual/perennial crops. The fragmentation process followed parameter values obtained from the BLB process, and size distributions were recorded at 1, 5, 10, 50, 100, 200, 500, and 1000 years of evolution. This analysis isolates the effect of the size-dependent fragmentation from the confounding influence of continuous emission inputs, thus reveals the inherent redistribution patterns of particle numbers across size classes at extremely long timescales.

Sensitivity analysis

We conducted a local sensitivity analysis using a one-at-a-time approach to evaluate the model's sensitivity to each optimized parameter. For each optimized parameter, we applied perturbations of ±1%, ±5% and ±10% relative to its baseline (median value from the bootstrapping samples) while keeping all other parameters constant. We then calculated the relative changes of the loss function. This allowed us to check the stability of the results and identify which parameters dominate the model performance when pushed away from their optimal values.

As we applied data imputation for a substantial proportion of data entries, we assessed how this affected our findings. This was done as rerunning the parameter optimization process on high-quality subsets without missing planting histories or without missing lower bounds of particle size. We used the primary optimization results as initial values, and performed L-BFGS-B algorithm for each high-quality subset. The convergence threshold was set as 10^{-10} for higher precision and avoid falling into nearby parameter sets. The results were then compared against the optimization on the entire dataset.

Case study: MP accumulation by mulching in China

We use China as a case study to test our model on the MP accumulation from mulching. The use of plastic mulch films in China have expanded more than three folds over the past three decades[72] (Figure S9). Based on provincial-level data from the China Rural Statistical Yearbooks (Department of Rural Socioeconomic Survey, 1994–2024), we simulated the historical MP accumulation caused by mulching in agricultural soils across China from 1993 to 2050. For each province, the proportion of mulched cropland area was linked to the dominant Köppen climate types of major farming regions (Table S11; Figure S10), which were used to determine the climate conditions in the model. We assumed that plastic mulch films were applied exclusively to annual cropping systems given their primary use in crops such as maize, cotton, and vegetables. To project future trends, three scenarios were defined as: (1) Business as Usual, where the future mulching input intensity was set as the mean values of 2020–2024; (2) Moderate Mulching Residuals, where the future mulching residuals in croplands was 50% of the Business-as-Usual scenario; and (3) No Mulching Residuals, representing a complete removal of new MP inputs from mulching. For each scenario, we simulated the temporal evolution of MP accumulation across provinces and tracked the redistribution of particles across size classes.

Acknowledgement

The authors declare no competing interests. We thank Prof. Yanyan Zhang and Prof. Liang Lei for their profound and helpful suggestions to this work.

Author Contributions (following CReDIT)

SD, LL, & TCW conceptualized the work. SD wrote the first draft of the manuscript. All authors discussed the work at various stages of the research. All authors revised later versions of the manuscript. LL & TCW supervised the work. TCW secured project funding.

References

1. FAO. *Assessment of Agricultural Plastics and Their Sustainability: A Call for Action*. (Rome, 2021). doi:10.4060/cb7856en.
2. Rillig, M. C. & Lehmann, A. Microplastic in terrestrial ecosystems. *Science* **368**, 1430–1431 (2020).
3. Sheng, D. *et al.* Plastic pollution in agricultural landscapes: an overlooked threat to pollination, biocontrol and food security. *Nat. Commun.* **15**, 8413 (2024).
4. Garbounis, G., Karasali, H. & Komilis, D. Origin, Occurrence and Threats of Microplastics in Agricultural Soils: A Comprehensive Review. *Sustainability* **18**, 1524 (2026).
5. Lwanga, E. H. *et al.* Review of microplastic sources, transport pathways and correlations with other soil stressors: a journey from agricultural sites into the environment. *Chem. Biol. Technol. Agric.* **9**, 20 (2022).
6. Tian, L., Jinjin, C., Ji, R., Ma, Y. & Yu, X. Microplastics in agricultural soils: sources, effects, and their fate. *Curr. Opin. Environ. Sci. Health* **25**, 100311 (2022).
7. Zhang, L. *et al.* Atmospheric microplastic deposition in Guilin karst wetlands: Sources and agricultural impact. *Atmos. Pollut. Res.* **16**, 102537 (2025).
8. Zhao, H. *et al.* Microplastic pollution in organic farming development cannot be ignored in China: Perspective of commercial organic fertilizer. *J. Hazard. Mater.* **460**, 132478 (2023).
9. Zhu, K. *et al.* Long-term phototransformation of microplastics under simulated sunlight irradiation in aquatic environments: Roles of reactive oxygen species. *Water Res.* **173**, 115564 (2020).
10. Song, Y. K. *et al.* Combined Effects of UV Exposure Duration and Mechanical Abrasion on Microplastic Fragmentation by Polymer Type. *Environ. Sci. Technol.* **51**, 4368–4376 (2017).
11. Moyal, J. *et al.* Impacts of Biofilm Formation on the Physicochemical Properties and Toxicity of Microplastics: A Concise Review. *Rev. Environ. Contam. Toxicol.* **261**, 8 (2023).
12. Liu, Z., Liu, H., Wang, L. & Zhang, J. Decreased particle size enhances the aging behavior of microplastics during sewage sludge composting: Physicochemical properties and cadmium loading. *J. Hazard. Mater.* **490**, 137779 (2025).
13. Özdemir, S. *et al.* Isolation of Thermophilic Bacteria and Investigation of Their Microplastic Degradation Ability Using Polyethylene Polymers. *Microorganisms* **10**, 2441 (2022).
14. Zhang, X. *et al.* Time-dependent effects of microplastics on soil bacteriome. *J. Hazard. Mater.* **447**, 130762 (2023).
15. Su, X. *et al.* Comprehensive Understanding on the Aging Process and Mechanism of Microplastics in the Sediment–Water Interface: Untangling the Role of Photoaging and Biodegradation. *Environ. Sci. Technol.* **58**, 16164–16174 (2024).
16. Gusli, S., Cass, A., Macleod, D. A. & Blackwell, P. S. Structural collapse and strength of some Australian soils in relation to hard setting: I. Structural collapse on wetting and draining. *Eur. J. Soil Sci.* **45**, 15–21 (1994).
17. Berenstein, G. *et al.* Macro, meso, micro and nanoplastics in horticultural soils in Argentina: Abundance, size distribution and fragmentation mechanism. *Sci. Total Environ.* **906**, 167672 (2024).
18. Hino, S., Kawasaki, N., Yamano, N., Nakamura, T. & Nakayama, A. Effects of particle size on marine biodegradation of poly(l-lactic acid) and poly(ε-caprolactone). *Mater. Chem. Phys.* **303**, 127813 (2023).

19. Fang, Z., Sallach, J. B. & Hodson, M. E. Size- and concentration-dependent effects of microplastics on soil aggregate formation and properties. *J. Hazard. Mater.* **465**, 133395 (2024).
20. Li, H., Liu, L. & Li, C. Small-size polyethylene and polylactic microplastic alterations on soil aggregate formation with soil sterilization. *Chemosphere* **364**, 143158 (2024).
21. Ju, T. *et al.* Microplastics sequestered in the soil affect the turnover and stability of soil aggregates: A review. *Sci. Total Environ.* **904**, 166776 (2023).
22. Liu, Y. *et al.* Transport and transformation of microplastics and nanoplastics in the soil environment: A critical review. *Soil Use Manag.* **37**, 224–242 (2021).
23. George, M., Nallet, F. & Fabre, P. A threshold model of plastic waste fragmentation: New insights into the distribution of microplastics in the ocean and its evolution over time. *Mar. Pollut. Bull.* **199**, 116012 (2024).
24. Meizoso-Regueira, T., Fuentes, J., Cusworth, S. J. & Rillig, M. C. Prediction of future microplastic accumulation in agricultural soils. *Environ. Pollut.* **359**, 124587 (2024).
25. Kaandorp, M. L. A., Dijkstra, H. A. & Van Sebille, E. Modelling size distributions of marine plastics under the influence of continuous cascading fragmentation. *Environ. Res. Lett.* **16**, 054075 (2021).
26. Pérez-Muñuzuri, V. Size-Dependent Microplastic Fragmentation Model. *J. Mar. Sci. Eng.* **12**, 1213 (2024).
27. Quik, J. T. K., Meesters, J. A. J. & Koelmans, A. A. A multimedia model to estimate the environmental fate of microplastic particles. *Sci. Total Environ.* **882**, 163437 (2023).
28. Wang, L. *et al.* Modeling the Conditional Fragmentation-Induced Microplastic Distribution. *Environ. Sci. Technol.* **55**, 6012–6021 (2021).
29. Liang, M. *et al.* China's agricultural plastic mulch transition is a food security imperative with global implications. *Nat. Food* **7**, 113–114 (2026).
30. Corradini, F. *et al.* Evidence of microplastic accumulation in agricultural soils from sewage sludge disposal. *Sci. Total Environ.* **671**, 411–420 (2019).
31. Miao, H. *et al.* Microplastics occurrence and distribution characteristics in mulched agricultural soils of Guizhou province. *Sci. Rep.* **14**, 21505 (2024).
32. Zhang, S., Bao, A., Lin, X., Jia, G. & Zhang, Q. Microplastic Accumulation in Agricultural Soils with Different Mulching Histories in Xinjiang, China. *Sustainability* **15**, 5438 (2023).
33. FAO. *State of Research on the Impacts of Plastic Pollution on Soil Health and Crops*. (FAO, 2025). doi:10.4060/cd6407en.
34. El-Beltagi, H. S. *et al.* Mulching as a Sustainable Water and Soil Saving Practice in Agriculture: A Review. *Agronomy* **12**, 1881 (2022).
35. Pechlivanis, N. *et al.* Microbial co-occurrence network demonstrates spatial and climatic trends for global soil diversity. *Sci. Data* **11**, 672 (2024).
36. Turcotte, D. L. Fractals and fragmentation. *J. Geophys. Res. Solid Earth* **91**, 1921–1926 (1986).
37. Zhang, G. S. & Liu, Y. F. The distribution of microplastics in soil aggregate fractions in southwestern China. *Sci. Total Environ.* **642**, 12–20 (2018).
38. Schefer, R. B., Koestel, J. & Mitrano, D. M. Minimal vertical transport of microplastics in soil over two years with little impact of plastics on soil macropore networks. *Commun. Earth Environ.* **6**, 278 (2025).
39. Liao, J. & Chen, Q. Biodegradable plastics in the air and soil environment: Low degradation rate and high microplastics formation. *J. Hazard. Mater.* **418**, 126329 (2021).

40. Huang, Y., Liu, Q., Jia, W., Yan, C. & Wang, J. Agricultural plastic mulching as a source of microplastics in the terrestrial environment. *Environ. Pollut.* **260**, 114096 (2020).
41. Liu, B., Li, W., Pan, X. & Zhang, D. The persistently breaking trade-offs of three-decade plastic film mulching: Microplastic pollution, soil degradation and reduced cotton yield. *J. Hazard. Mater.* **439**, 129586 (2022).
42. Fu, F. *et al.* Combined pollution and soil microbial effect of pesticides and microplastics in greenhouse soil of suburban Tianjin, Northern China. *Environ. Pollut.* **340**, 122898 (2024).
43. Rana, Md. M., Haque, Md. R., Tasnim, S. S. & Rahman, Md. M. The potential contribution of microplastic pollution by organic fertilizers in agricultural soils of Bangladesh: quantification, characterization, and risk appraisals. *Front. Environ. Sci.* **11**, 1205603 (2023).
44. Zhang, S. *et al.* Occurrence and distribution of microplastics in organic fertilizers in China. *Sci. Total Environ.* **844**, 157061 (2022).
45. Üstün, G. E., Bozdaş, K. & Can, T. Abundance and characteristics of microplastics in an urban wastewater treatment plant in Turkey. *Environ. Pollut.* **310**, 119890 (2022).
46. Panahi Fard, M. *et al.* Microplastics in MSW-derived compost: release rate, characteristics, ecological risks, and mitigation strategies for sustainable agriculture. *Environ. Pollut. Bioavailab.* **37**, 2529998 (2025).
47. Qiu, Q. *et al.* An Evaluation of Potential Microplastic Risk from Commercial Organic Fertilizers. *Waste Biomass Valorization* **17**, 247–256 (2026).
48. Hamza, M. *et al.* Variation in microplastic characteristics during biosolid stabilization across wastewater resource recovery facilities in the United States and Canada. *J. Environ. Manage.* **397**, 128374 (2026).
49. Pérez-Reverón, R. *et al.* Recycled wastewater as a potential source of microplastics in irrigated soils from an arid-insular territory (Fuerteventura, Spain). *Sci. Total Environ.* **817**, 152830 (2022).
50. Jiang, J.-J. *et al.* Current levels and composition profiles of microplastics in irrigation water. *Environ. Pollut.* **318**, 120858 (2023).
51. Ben-David, E. A. *et al.* Microplastic distributions in a domestic wastewater treatment plant: Removal efficiency, seasonal variation and influence of sampling technique. *Sci. Total Environ.* **752**, 141880 (2021).
52. Brahney, J. *et al.* Constraining the atmospheric limb of the plastic cycle. *Proc. Natl. Acad. Sci.* **118**, e2020719118 (2021).
53. Ertürk Arı, P. *et al.* Atmospheric microplastic dispersion in diverse land-use context: insight from the black sea coastal region in Türkiye. *Air Qual. Atmos. Health* **18**, 1729–1743 (2025).
54. Du, A. *et al.* Distribution Characteristics of Atmospheric Microplastics in Typical Desert Agricultural Regions. *Environ. Toxicol. Chem.* **43**, 1982–1995 (2024).
55. Mutshekwa, T. *et al.* Atmospheric deposition of microplastics in urban, rural, forest environments: A case study of Thulamela Local Municipality. *PLOS ONE* **20**, e0313840 (2025).
56. Szewc, K., Graca, B. & Dołęga, A. Atmospheric deposition of microplastics in the coastal zone: Characteristics and relationship with meteorological factors. *Sci. Total Environ.* **761**, 143272 (2021).
57. Chen, Y. *et al.* Quantification and Characterization of Fine Plastic Particles as Considerable Components in Atmospheric Fine Particles. *Environ. Sci. Technol.* **58**, 4691–4703 (2024).
58. Liao, Z. *et al.* Airborne microplastics in indoor and outdoor environments of a coastal city in Eastern China. *J. Hazard. Mater.* **417**, 126007 (2021).

59. Zhu, J. *et al.* Atmospheric deposition is an important pathway for inputting microplastics: Insight into the spatiotemporal distribution and deposition flux in a mega city. *Environ. Pollut.* **341**, 123012 (2024).
60. Beaurepaire, M., Gasperi, J., Tassin, B. & Dris, R. COVID lockdown significantly impacted microplastic bulk atmospheric deposition rates. *Environ. Pollut.* **344**, 123354 (2024).
61. Klein, M. & Fischer, E. K. Microplastic abundance in atmospheric deposition within the Metropolitan area of Hamburg, Germany. *Sci. Total Environ.* **685**, 96–103 (2019).
62. Lu, L. *et al.* Occurrence, influencing factors and sources of atmospheric microplastics in peri-urban farmland ecosystems of Beijing, China. *Sci. Total Environ.* **912**, 168834 (2024).
63. Jafarova, M., Aherne, J. & Loppi, S. Regional sources drive atmospheric microplastic deposition at rural background sites. *Environ. Res.* **285**, 122663 (2025).
64. Luqman, M. *et al.* Quantification and characterization of microplastics (MPs) pollution in peri-uburban agricultural lands of Lahore, Pakistan. *PLOS ONE* **18**, e0291760 (2023).
65. Huber, P. J. Robust Estimation of a Location Parameter. *Ann. Math. Stat.* **35**, 73–101 (1964).
66. Xiang, Y., Sun, D. Y., Fan, W. & Gong, X. G. Generalized simulated annealing algorithm and its application to the Thomson model. *Phys. Lett. A* **233**, 216–220 (1997).
67. Zhu, C., Byrd, R. H., Lu, P. & Nocedal, J. Algorithm 778: L-BFGS-B: Fortran subroutines for large-scale bound-constrained optimization. *ACM Trans. Math. Softw.* **23**, 550–560 (1997).
68. Kleiner, A., Talwalkar, A., Sarkar, P. & Jordan, M. I. A Scalable Bootstrap for Massive Data. *J. R. Stat. Soc. Ser. B Stat. Methodol.* **76**, 795–816 (2014).
69. Wang, Y. *et al.* A case on source to soil to solutions: Distribution characteristics of microplastics in farmland soil of the largest vegetable base in Northwest China. *Sci. Total Environ.* **907**, 167910 (2024).
70. Cao, J. *et al.* Distribution characteristics and correlation of macro- and microplastics under long-term plastic mulching in northwest China. *Soil Tillage Res.* **231**, 105738 (2023).
71. Xu, T., Zheng, S., Duo, X., Hou, Z. & Wu, J. Long-term plastic mulching exacerbates the co-limitation of carbon and phosphorus in farmland by altering physicochemical properties and microbial interactions. *Front. Microbiol.* **16**, 1694370 (2026).
72. Liu, E. K., He, W. Q. & Yan, C. R. ‘White revolution’ to ‘white pollution’—agricultural plastic film mulch in China. *Environ. Res. Lett.* **9**, 091001 (2014).
73. Department of Rural Socioeconomic Survey. China rural statistical yearbook. China Statistics Press (2024).

Tables and figures

Table 1. Current models on microplastic fragmentation

Target system	Size-dependent	Temporal evolution	Mechanism interpretation	Empirical validation	Publication
Marine	√	√	×	×	George et al.[23]
Marine	√	√	×	×	P.-M.[26]
Terrestrial	×	√	√	√	Quik et al.[27]
Terrestrial	√	×	×	√	Wang et al. [28]
Agriculture	×	√	×	√	M.-R. et al.[24]
Marine	√	√	√	√	Kaarndop et al.[25]
Agricultural	√	√	√	√	This work

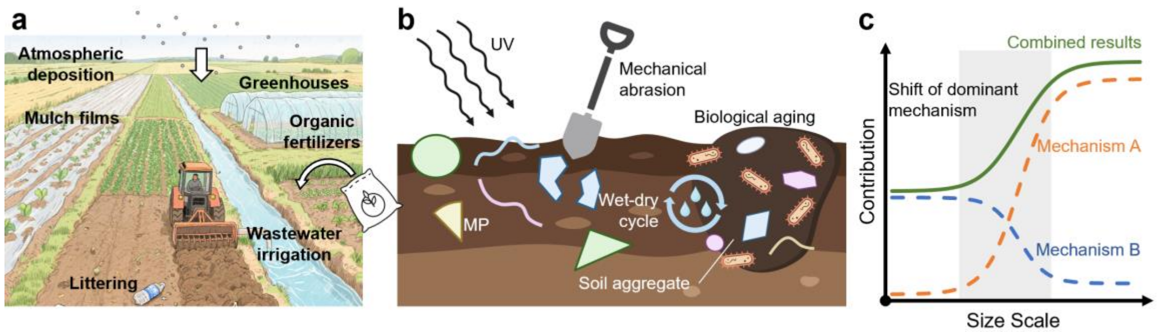

Figure 1. Conceptual framework of MP input sources and fragmentation processes in farmland soils. (a) Potential pathways introducing MP into farmland soils include atmospheric deposition, plastic mulch films, plastic greenhouses, applications of organic fertilizers, wastewater irrigation, and unmanaged littering. **(b)** Size-dependent MP aging and fragmentation drivers in the farmland soil profile. In the bulk soil matrix, large MPs are primarily influenced by UV-driven photoaging and macro-scale mechanical abrasion from tillage. As particle size decreases and MPs become incorporated into soil aggregates, biotic aging and micro-stresses induced by wet-dry cycles increasingly govern the dynamics. **(c)** Conceptual representation of the modelling framework where multiple mechanisms contribute to the same environmental process and the relative importance of different mechanism shifts over spatial scale. Mechanism A in dashed orange line (e.g., photoaging) and B in dashed blue line (e.g., biological aging) both contribute to MP fragmentation in agricultural soils, and both changes depending on the size of MP particles. As a result, the observed fragmentation rate also changes in solid green line. The modelling framework captures this aggregate response through a unified effective parameter rather than explicitly resolving each mechanism. Note: the background illustration of panel (a) was generated by Doubao (ByteDance).

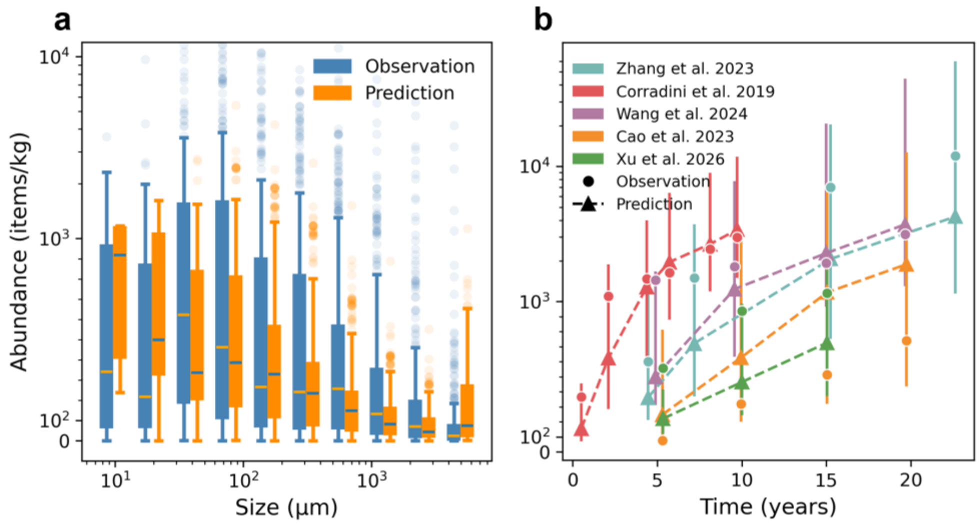

Figure 2. Model predictions and observations. (a) Comparing on the complete dataset. Boxplot of observed MP abundance and median values of predicted distribution across particle size classes. For each observational data, we only plot the median value of the predicted distribution from bootstrapping. The median value of each box is shown as a horizontal line. Whiskers extend to the 5–95% intervals of boxes. **(b)** Validation against time-series data from literature. Model prediction coverage reached 90.48% on five agricultural sites over the span of more than 20 years.[30,32,69–71] Solid lines with circles denote observational data; dashed line with triangles denote median values of simulated data, and error bars cover the 95% prediction intervals.

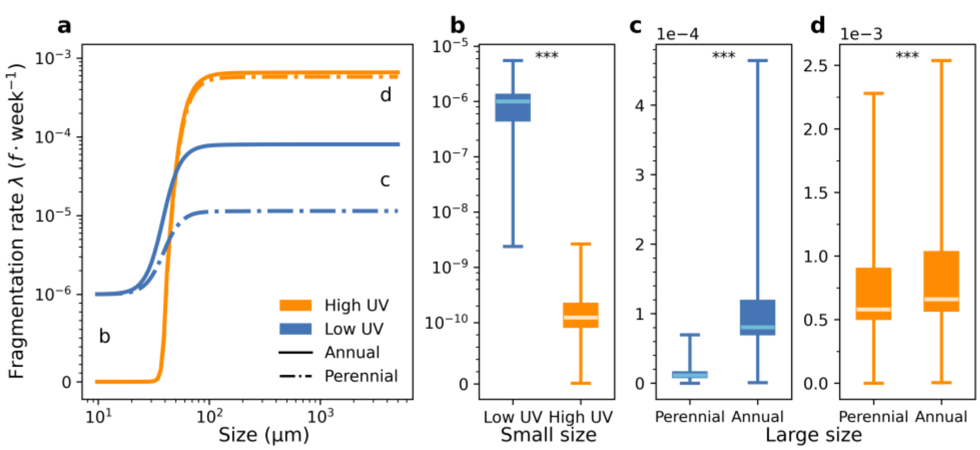

Figure 3. Size-dependent fragmentation rates under different climate types and cropping systems. (a) Median values of fragmentation rates against MP sizes. Orange lines represent high-UV climates and blue ones represent low-UV climates. Annual crop sites are plotted in solid lines, and perennial sites in dash-dot lines. **(b)–(d)** Boxplots of the limits of fragmentation rates for small MPs under different climate conditions, and for large MPs across climate conditions combined with cropping cycles. The median value of each box is shown as a horizontal line. Whiskers extend to the 5–95% intervals of boxes. *** $p < 0.001$ (Bonferroni-adjusted Mann-Whitney U Test).

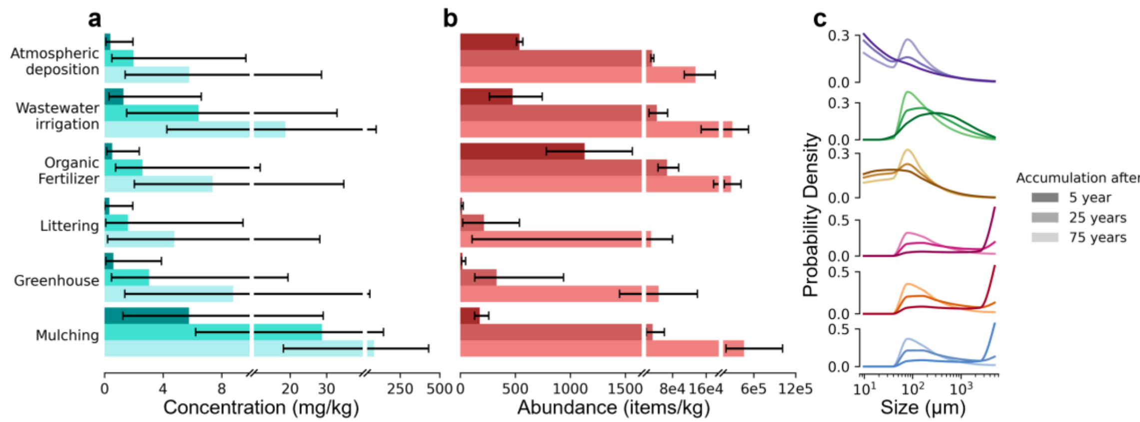

Figure 4. Simulated MP accumulation in annual crop sites under high UV climates after 5, 25 and 75 years (from 2025 to 2030, 2050 and 2100) of different continuous inputs. (a) MP mass concentrations (mg/kg) for different sources (atmospheric deposition, wastewater irrigation, organic fertilizer application, unmanaged littering, plastic greenhouses and mulch films). **(b)** Corresponding particle abundances (items/kg). Bars denote median values and error bars indicate the interquartile range (Q1–Q3) derived from bootstrap simulations. **(c)** The evolution of size distributions (probability density functions, PDF) for each source, shown as the median values of model simulation. Color gradients in each panel represents the time periods of simulation, where the darkest shades stand for 5 years, moderate shades for 25 years, and light shades for 75 years.

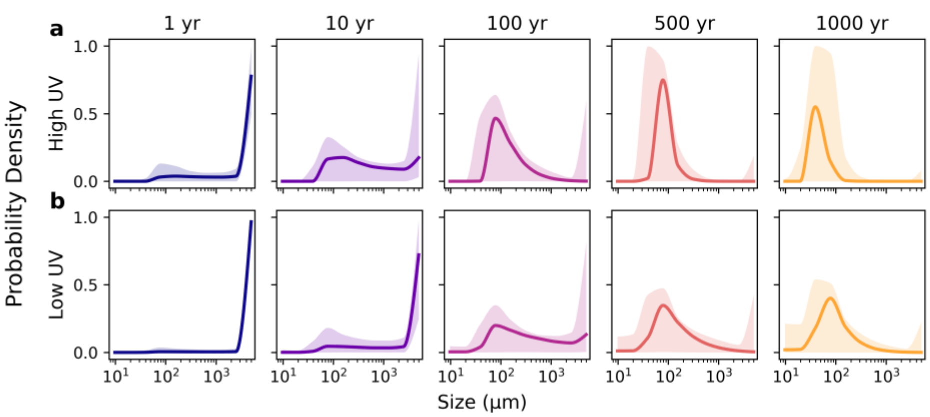

Figure 5. Simulated theoretical evolution of MP size distributions for a single parent particle (5 mm) under (a) high- and (b) low-UV climates in an annual crop site. Curves represent the median relative abundance across size classes after 1, 10, 100, 500, and 1000 years, and shaded bands indicate the 5–95% uncertainty.

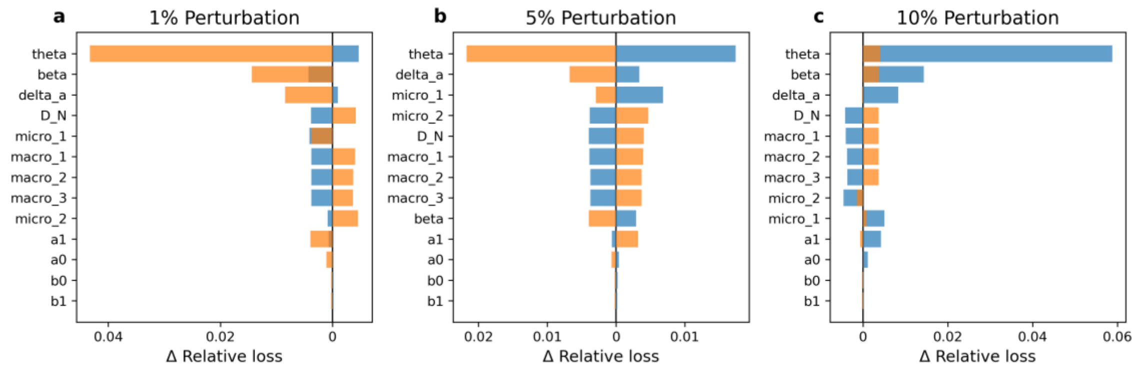

Figure 6. Tornado plot of model sensitivity at perturbations of (a) ±1%, (b) ±5% and (c) ±10% for each optimized parameter. Blue bars represent the changes in relative loss values from positive perturbations on parameters, and orange bars represent the changes from negative perturbations.

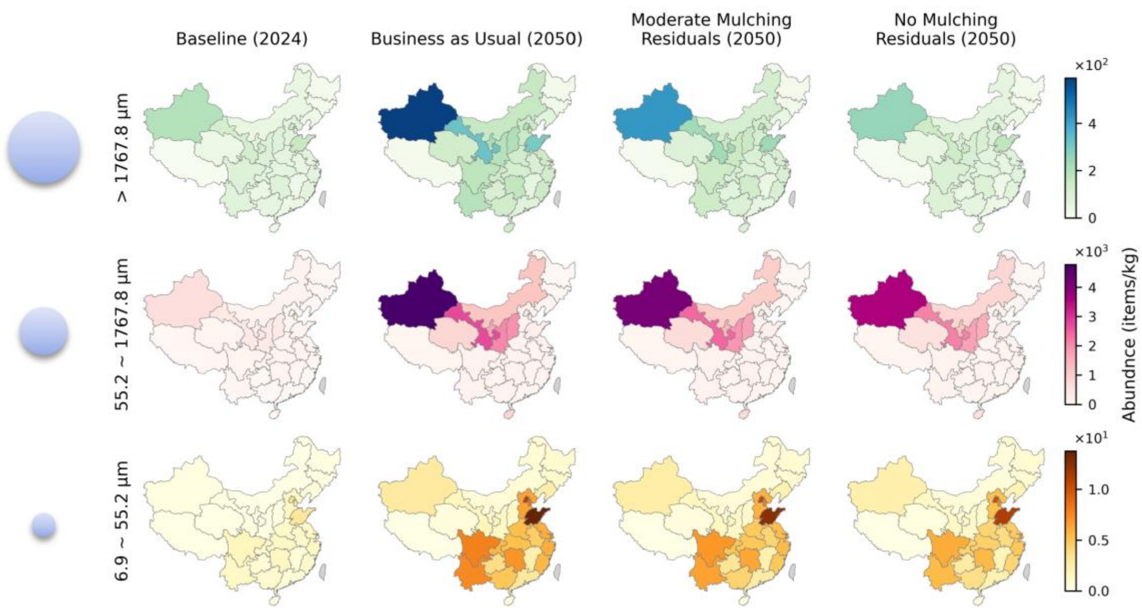

Figure 7. Provincial-level projections of MP accumulation in Chinese agricultural soils derived from plastic mulch films. The first column represents the baseline condition in 2024, and the other three projections for 2050 including Business as Usual, Moderate Mulching Residuals (50% reduction of residual inputs), and No Mulching Residuals. Rows represent different particle size classes (> 1767.8 µm, 55.2–1767.8 µm, and 6.9–55.2 µm). Colors indicate simulated values of MP abundance (items/kg) within agricultural soils.

Box 1. Future Research Directions towards a comprehensive plastic pollution modelling approach for agricultural soils

i) Quantifying micro-scale mechanisms of MP fragmentation. In particular, wetting–drying cycles within soil aggregates may generate repeated mechanical stress capable of fragmenting MPs over long timescales. Similarly, biotic aging driven by microbial activity may alter polymer surfaces and accelerate subsequent fragmentation. Quantifying these processes experimentally would provide valuable constraints for future models.

ii) Expanding detection limits of analytical techniques for plastic pollution. Current measurement methods often have detection limits at tens or hundreds of micrometers, whereas fragmentation models suggest that large MPs may continuously generate much smaller particles. Improved detection technologies would therefore help validate fragmentation models and better characterize the full spectrum of MP sizes in soils.

iii) Developing remediation strategies to handle legacy MPs in agricultural soils. As we show that large plastic fragments remain from historical MP pollution, developing specific removal tools of plastic fragments such as *in-situ* biodegradation agents is critical to minimize future MP impacts on agricultural landscapes and food systems.

iv) Linking MPs in agricultural soils to crop production and regulating ecosystem services. Future work should assess the ecotoxicological effects of MPs on soil organisms and crop systems, and explore the potential development of crop varieties that are more tolerant to MP-contaminated soils.

Supplementary Information for

Microplastics in farmlands: A model of conditional fragmentation and source estimation

Dong Sheng[1,2,3*], Feng Ju[4], Ling Li[2†], Thomas Cherico Wanger[3,5*†]

1. College of Environmental and Resource Sciences, Zhejiang University, Hangzhou 310058, China
2. Key Laboratory of Coastal Environment and Resources of Zhejiang Province, School of Engineering, Westlake University, Hangzhou 310030, China
3. Production Technology and Diversified Cropping Systems Group, Agroscope, Nyon 1260, Switzerland
4. Environmental Microbiome and Biotechnology Laboratory, Center of Synthetic Biology and Integrated Bioengineering, School of Engineering, Westlake University, Hangzhou 310030, China
5. Academy of Global Food Economics and Policy, China Agricultural University, Beijing 100083, China

* Correspondence: DS(shengdong@westlake.edu.cn), TCW(tomcwanger@gmail.com)
† These authors jointly supervised this work

Supplementary Methods

Method S1. Handling missing planting years

We used the empirical modal range (central 20–80% percentile range) of known planting histories in our dataset (Figure S6) to infer the potential minimum and maximum planting years of unknown sites. The criteria are as follows:

1. For all data with unknown planting histories, the default range is 6.4–22.5 years, which is the majority of available site planting histories in our dataset (Figure S6a);
2. If a site applied mulching, we infer its planting history as 7–22.5, as this is the main range for mulching sites with known planting histories (Figure S6b);
3. Plastic greenhouses suggest a planting history of 8.7–19.6 years, as indicated in our dataset (Figure S6c);
4. If organic fertilizers have been applied, we infer that the planting years of the site is 6–22.5 years (Figure S6d), which is relatively shorter because the practice of organic fertilization might be intervened by changing factors like policies, supplies, etc.;
5. The inferred planting histories for sites with poorly managed littering is set as 11.2–29.4 years (Figure S6e);
6. Compared to annual crop sites, perennial sites such as orchards tend to be managed more consistently. Thus, we add extra 5 years to the inferred minimum and maximum of inferred planting years.

When multiple rules are triggered simultaneously, we take the intersection of all ranges as the final inferred planting history.

Method S2. MP Particle Dimensions

From the 438 data entries collected from the literature, we retrieved 300 entries of MP particle shape data, such as fibers, films, pellets, fragments, and others. Based on their geometric features, each shape category was assigned a fixed particle dimensionality (D_N). Fibers and lines were assigned a D_N of 1, as their length is the dominant dimension. Films, sheets, and flakes were given a D_N of 2, since their thickness is substantially smaller than the length and width. Pellets, spheres, beads, and granules were assigned a D_N of 3, reflecting their similar or identical scales in all directions. Fragments were given a D_N of 2.5, as they exhibit irregular, asymmetrical shapes without any dimension being significantly smaller than the others. Foams were also assigned a D_N of 2 because the porous structure limits the fragmentation process to the 2-D surfaces of pore walls. Using these assignments, we calculated the weighted average particle dimension for each data entry (Figure S7). We set the D_N in our model to follow a uniform random distribution between 1.4–2.4, roughly covering the central 80% of the data.

Method S3. Formulation of the transition matrix

In our model, the temporal size distribution of MP is described as an array

$$\boldsymbol{Y}(t) = [y_{0,t} \quad y_{1,t} \quad y_{2,t} \quad \cdots \quad y_{k,t} \quad \cdots \quad y_{K,t}]^T$$

where $y_{k,t}$ is the MP mass at size class k at time t. After a timestep of Δt, we get a new size distribution $\boldsymbol{Y}(t+\Delta t)$. If we do not consider any external inputs, the new distribution would be completely determined by the fragmentation process. After Δt, particles at size class k_0 split off into a series of smaller particles,[1] and the mass proportion of child particles at size class k_e is

$$P_{k_0 \to k_e} = \frac{\Gamma(k_e - k_0 + \lambda\Delta t - 1)}{\Gamma(k_e - k_0 + 1) \cdot \Gamma(\lambda\Delta t)} \cdot p^{k_e - k_0} \cdot (1-p), \qquad (k_e \geq k_0)$$

Consider particles at size class k, the updated value is

$$y_{k,t+\Delta t} = P_{0\to k} \cdot y_{0,t} + P_{1\to k} \cdot y_{1,t} + \cdots + P_{k\to k} \cdot y_{k,t}$$

Therefore, we can formulate the Markov process as

$$\begin{bmatrix} y_{0,t+\Delta t} \\ y_{1,t+\Delta t} \\ y_{2,t+\Delta t} \\ \vdots \\ y_{k,t+\Delta t} \\ \vdots \\ y_{K,t+\Delta t} \end{bmatrix} = \begin{bmatrix} P_{0\to 0} & 0 & 0 & \cdots & 0 \\ P_{0\to 1} & P_{1\to 1} & 0 & \cdots & 0 \\ P_{0\to 2} & P_{1\to 2} & P_{2\to 2} & \cdots & 0 \\ \vdots & \vdots & \vdots & \ddots & \vdots \\ P_{0\to k} & P_{1\to k} & P_{2\to k} & \cdots & 0 \\ \vdots & \vdots & \vdots & \ddots & \vdots \\ P_{0\to K} & P_{1\to K} & P_{2\to K} & \cdots & P_{K\to K} \end{bmatrix} \times \begin{bmatrix} y_{0,t} \\ y_{1,t} \\ y_{2,t} \\ \vdots \\ y_{k,t} \\ \vdots \\ y_{K,t} \end{bmatrix}$$

i.e.,

$$\boldsymbol{Y}(t+\Delta t) = \boldsymbol{T} \cdot \boldsymbol{Y}(t)$$

where $\boldsymbol{T}$ is the dominating transition matrix under timestep Δt. To include external MP input sources, the input arrays is added onto $\boldsymbol{Y}(t)$ before the matrix multiplication:

$$\boldsymbol{Y}(t+\Delta t) = \boldsymbol{T} \cdot \left(\boldsymbol{Y}(t) + \sum_{i \in S} \alpha_i \cdot \mathbf{Input}_i \right)$$

which yields the same equation as (5) in the main text.

Method S4. Assessing vertical transports and mineralization

There are two main factors challenging the conservation of mass in our model: vertical downward transport and biological mineralization.

MPs in the top layers of soil may be vertically transported to deeper soil and eventually into underground waters. However, the speed of vertical transport is relatively slow. For instance, Zhao et al. reported that after 4 runs of irrigation (up to saturated state), only 0.2% of the total MP transported to the 40–50 cm soil layer.[2] Another experiment simulated 14 days of heavy rainfall (13 mm/h), and found only 0.6% of total MPs transported below 18 cm.[3] Realistic field trials in Switzerland also revealed a minimal vertical transport of MPs, with only ~1% reaching below 8 cm soil depth in two years,[4] which is roughly 22% in the top layer after 50 years. Given that the MP concentration in our dataset varies across more than 4 magnitudes, the mass loss is considered small and negligible. Therefore, we neglect the mass loss due to vertical transport in our model.

For biological mineralization, Chamas et al. proposed the concept of specific surface degradation rate (SSDR), whereby the perpendicular depth of plastic degradation per unit time is used to quantify microbial activities.[5] This allows for comparisons across different MP particle sizes and shapes. However, they likely over-estimated the reaction rates in soil profiles, as the literature data they adopted were mostly under controlled lab conditions and/or enriched MP-degrading microbes. Liao & Chen tested MP biodegradation under realistic field conditions for six months, and reported a weight loss of -0.1 ± 0.3% for non-biodegradable polyethylene films (thickness = 25 μm).[6] Based on geometric conversion, this corresponds to an annual surface degradation rate of 25 ± 75 nm per year. For a sphere-shaped MP particle at the smallest size class of our model (9.76 μm in diameter), this reaction rate translates to an annual mass loss of merely 0.26 ± 0.77%. The relative mass loss becomes even smaller for larger particle size classes. Therefore, the impact of biological mineralization on MP mass can also be neglected in our model.

Method S5. Poisson regression model as the benchmark

Meizoso-Regueira et al.[7] developed a statistical model to predict the accumulation of microplastics in agricultural soils. The model is based on Poisson regression

$$Y \sim Poisson(\lambda);\ \ \lambda = e^{\beta_0+\beta_1 x} = e^{\beta_0} \cdot \left(e^{\beta_1}\right)^x$$

where Y is the MP abundance (summed up from all size classes), e^{β_0} is the expected response of microplastic accumulation for time zero $x = 0$, and e^{β_1} is the expected rate of increase by unit of time x. The original model was performed on a long-term dataset of organic fertilizer applications, which is relatively simple. To adapt the model for our dataset with multiple input sources, we constructed the prediction equation as the sum of all sources, and allowed β_0 and β_1 to vary for each one.

$$\lambda = \sum_{i \in S} e^{\beta_{i,0}} \cdot \left(e^{\beta_{i,1}}\right)^{years}$$

We then constructed the loss function using the same Huber loss criteria, and optimized the parameters using the dual annealing algorithm. After obtaining the best parameter set, we compared the model performance using the same evaluation criteria of the process-based model of this work.

Supplementary Tables

Table S1. Model performance on the complete dataset, comparison to the regression-based benchmark model,[7] and validation on literature with time-series data. MedAE – median absolute errors; MAE – mean absolute errors.

	Complete dataset	Validation	Benchmark
Robust R^2 (Huber loss)	0.412	0.586	0.341
MedAE (items/kg)	200.49	425.64	5099.58
MedAE on logarithm*	1.48	0.68	2.04
MAE (items/kg)	1627.85	1024.27	15693.78
MAE on logarithm*	1.85	0.62	2.97
Pearson correlation	0.230	0.775	0.056
Prediction coverage†	43.18%	90.48%	NA
Number of observations	3235	21	438

* Logarithmic transformation with a shift of one, i.e., $\log_{10}(y+1)$.

† The coverage of 95% prediction intervals on observations.

Table S2. Summary of posterior distributions of optimized parameters from the BLB process. The table presents the median, first quartile (Q_1) third quartile (Q_3), and the 5th and 95th percentiles (PR_5 and PR_{95}, representing the 90% credible interval) for each parameter. For meanings of each parameter, see Table S10. The derived parameters $\boldsymbol{a_0}+\boldsymbol{\delta_a}$ and $\boldsymbol{a_1}+\boldsymbol{\delta_a}$, as defined in equation $(\mathbf{4})$, are also included.

Parameter	Median	Q_1	Q_3	PR_5	PR_{95}
`a0`	1.15×10^{-5}	8.29×10^{-6}	1.61×10^{-5}	2.42×10^{-8}	6.98×10^{-5}
`a1`	5.81×10^{-4}	5.04×10^{-4}	9.03×10^{-3}	3.68×10^{-7}	2.29×10^{-3}
`delta_a`	6.85×10^{-5}	5.57×10^{-5}	9.97×10^{-5}	2.84×10^{-8}	3.65×10^{-4}
`a0 + delta_a`	8.05×10^{-5}	6.98×10^{-5}	1.19×10^{-4}	8.26×10^{-7}	4.65×10^{-4}
`a1 + delta_a`	6.60×10^{-4}	5.69×10^{-4}	1.03×10^{-3}	4.42×10^{-6}	2.54×10^{-3}
`b0`	1.00×10^{-6}	4.49×10^{-7}	1.34×10^{-6}	2.36×10^{-9}	5.56×10^{-6}
`b1`	1.23×10^{-10}	9.28×10^{-11}	2.23×10^{-10}	1.31×10^{-12}	2.69×10^{-9}
`theta`	7.05	6.97	7.12	5.58	7.53
`beta`	3.81	3.73	3.97	2.90	4.57
`macro_1`	0.381	0.326	0.493	0.072	0.795
`macro_2`	0.037	0.027	0.100	0.000	0.409
`macro_3`	0.038	0.003	0.047	0.000	0.214
`micro_1`	0.034	0.026	0.049	0.013	0.091
`micro_2`	0.117	0.064	0.154	0.000	0.299

Table S3. Simulated MP accumulation from different input sources in annual crop sites under high-UV climates after 5, 25 and 75 years, measured in mass concentration (mg/kg) and particle abundance (×10^3 items/kg). Results are reported as the median value followed by the interquartile range (Q1–Q3) in brackets.

	Concentration (mg/kg)			Abundance (×10^3 items/kg)		
	5 years	25 years	75 years	5 years	25 years	75 years
Mulch films	5.8 (1.3, 29.1)	28.7 (6.2, 144)	84.2 (18.1, 430)	0.2 (0.1, 0.3)	3.2 (1.7, 6)	46.1 (20.3, 101)
Greenhouse	0.6 (0.1, 3.9)	3.1 (0.5, 19.4)	8.8 (1.4, 57.4)	0.02 (0.01, 0.05)	0.3 (0.1, 0.9)	4.7 (1.4, 13.9)
Littering	0.3 (0, 1.9)	1.6 (0.1, 9.5)	4.8 (0.2, 28.1)	0.01 (0, 0.03)	0.2 (0, 0.5)	2.9 (0.1, 8)
Organic fertilizer	0.5 (0.2, 2.4)	2.6 (0.8, 11.8)	7.4 (2, 34.7)	1.1 (0.8, 1.6)	6.7 (4.6, 9.4)	27.4 (17.8, 41.8)
Wastewater irrigation	1.3 (0.3, 6.6)	6.4 (1.5, 32.8)	18.7 (4.3, 97.3)	0.5 (0.3, 0.7)	4.3 (2.4, 6.8)	29.2 (14.8, 52.5)
Atmospheric deposition	0.4 (0.1, 1.9)	2 (0.5, 9.6)	5.8 (1.4, 28.6)	0.5 (0.5, 0.6)	3.1 (2.9, 3.5)	13.5 (10.8, 18.2)

Table S4. Simulated MP accumulation from different input sources in annual crop sites under low-UV climates after 5, 25 and 75 years, measured in mass concentration (mg/kg) and particle abundance (×10^3 items/kg). Results are reported as the median value followed by the interquartile range (Q1–Q3) in brackets.

	Concentration (mg/kg)			Abundance (×10^3 items/kg)		
	5 years	25 years	75 years	5 years	25 years	75 years
Mulch films	5.8 (1.3, 29)	28.8 (6.3, 144)	86.3 (18.8, 432)	0.1 (0.1, 0.1)	0.8 (0.6, 1.1)	4.1 (2.6, 7.2)
Greenhouse	0.6 (0.1, 3.9)	3.1 (0.5, 19.4)	9.2 (1.5, 58.2)	0.01 (0.01, 0.03)	0.08 (0.05, 0.22)	0.4 (0.2, 1.3)
Littering	0.3 (0, 1.9)	1.6 (0.1, 9.7)	4.9 (0.2, 28.9)	0.01 (0, 0.01)	0.07 (0.01, 0.12)	0.3 (0.04, 0.7)
Organic fertilizer	0.5 (0.2, 2.4)	2.7 (0.8, 11.8)	7.9 (2.3, 35.4)	1.1 (0.8, 1.5)	5.6 (3.9, 7.8)	18.3 (12.9, 25.7)
Wastewater irrigation	1.3 (0.3, 6.6)	6.5 (1.5, 33)	19.4 (4.6, 98.8)	0.4 (0.2, 0.7)	2.3 (1.3, 3.7)	9.4 (4.9, 15.4)
Atmospheric deposition	0.4 (0.1, 1.9)	2 (0.5, 9.7)	6.1 (1.5, 29.1)	0.5 (0.5, 0.5)	2.7 (2.5, 2.8)	8.5 (8, 9.2)

Table S5. Simulated MP accumulation from different input sources in perennial crop sites under high-UV climates after 5, 25 and 75 years, measured in mass concentration (mg/kg) and particle abundance (×10^3 items/kg). Results are reported as the median value followed by the interquartile range (Q1–Q3) in brackets.

	Concentration (mg/kg)			Abundance (×10^3 items/kg)		
	5 years	25 years	75 years	5 years	25 years	75 years
Mulch films	5.8 (1.3, 29.1)	28.7 (6.2, 145)	85.1 (18.3, 431)	0.2 (0.1, 0.2)	2.7 (1.5, 5.2)	37.3 (16.1, 82.5)
Greenhouse	0.6 (0.1, 3.9)	3.1 (0.5, 19.4)	8.9 (1.4, 57.7)	0.02 (0.01, 0.04)	0.3 (0.1, 0.8)	3.7 (1.2, 10.6)
Littering	0.3 (0, 1.9)	1.6 (0.1, 9.5)	4.8 (0.2, 28.3)	0.01 (0, 0.02)	0.2 (0.02, 0.5)	2.3 (0.1, 6.4)
Organic fertilizer	0.5 (0.2, 2.4)	2.6 (0.8, 11.8)	7.5 (2.1, 34.8)	1.1 (0.8, 1.6)	6.4 (4.6, 9.3)	25.8 (17, 39.5)
Wastewater irrigation	1.3 (0.3, 6.6)	6.4 (1.5, 32.8)	18.9 (4.3, 97.7)	0.5 (0.2, 0.8)	4 (2.1, 6.7)	27 (12.5, 48.3)
Atmospheric deposition	0.1 (0.03, 0.6)	0.7 (0.2, 3.2)	2 (0.5, 9.4)	0.2 (0.2, 0.2)	1 (0.9, 1.1)	4.2 (3.4, 5.6)

Table S6. Simulated MP accumulation from different input sources in perennial crop sites under low-UV climates after 5, 25 and 75 years, measured in mass concentration (mg/kg) and particle abundance (×10^3 items/kg). Results are reported as the median value followed by the interquartile range (Q1–Q3) in brackets.

	Concentration (mg/kg)			Abundance (×10^3 items/kg)		
	5 years	25 years	75 years	5 years	25 years	75 years
Mulch films	5.8 (1.3, 29)	28.8 (6.3, 145)	86.5 (18.9, 432)	0.1 (0.1, 0.1)	0.6 (0.5, 0.7)	2.0 (1.6, 2.7)
Greenhouse	0.6 (0.1, 3.9)	3.1 (0.5, 19.4)	9.2 (1.5, 58.3)	0.01 (0.01, 0.03)	0.1 (0.04, 0.2)	0.2 (0.1, 0.6)
Littering	0.3 (0.02, 1.9)	1.6 (0.1, 9.7)	4.9 (0.2, 29)	0.01 (0, 0.01)	0.1 (0, 0.1)	0.2 (0.02, 0.3)
Organic fertilizer	0.5 (0.2, 2.4)	2.7 (0.8, 11.8)	8 (2.3, 35.5)	1.1 (0.8, 1.5)	5.5 (3.8, 7.5)	16.9 (11.6, 23.3)
Wastewater irrigation	1.3 (0.3, 6.6)	6.5 (1.5, 33)	19.5 (4.6, 99)	0.4 (0.2, 0.6)	2 (1.1, 3.3)	6.4 (3.5, 10.7)
Atmospheric deposition	0.1 (0.03, 0.7)	0.7 (0.2, 3.3)	2.1 (0.5, 9.8)	0.2 (0.2, 0.2)	0.9 (0.8, 0.9)	2.6 (2.5, 2.8)

Table S7. Comparison of parameters optimized on the entire dataset (median values), the subset without missing particle size lower bounds, the subset without missing planting histories, and the subset excluding all missing data entries. For meanings of each parameter see Table S10.

Dataset / Parameter	Entire dataset	No missing lower bounds	No missing planting histories	No missing data
a0	1.15×10^{-5}	1.18×10^{-5}	1.17×10^{-5}	1.17×10^{-5}
a1	5.81×10^{-4}	5.48×10^{-4}	5.66×10^{-4}	5.66×10^{-4}
delta_a	6.85×10^{-5}	6.75×10^{-5}	6.72×10^{-5}	6.71×10^{-5}
b0	1.00×10^{-6}	1.13×10^{-6}	1.14×10^{-6}	1.15×10^{-6}
b1	1.23×10^{-10}	1.25×10^{-10}	1.24×10^{-10}	1.24×10^{-10}
theta	7.05	7.05	7.05	7.05
beta	3.81	3.81	3.80	3.80
macro_1	0.381	0.414	0.423	0.423
macro_2	0.037	0.086	0.086	0.085
macro_3	0.038	0.092	0.090	0.091
micro_1	0.034	0.083	0.059	0.059
micro_2	0.117	0.168	0.168	0.169

Table S8. Overview of collected data entries across countries and climate conditions.

Climate	High UV					Low UV				Total
Country	Am	Aw	Bw	Bs	Cs	Cf	Cw	Df	Dw	
China	.	14	25	53	.	138	27	.	91	348
Bangladesh	8	10	.	.	.	.	.	.	.	18
India	9	7	.	1	.	1	.	.	.	18
Pakistan	.	.	10	4	.	.	.	.	.	14
Australia	.	.	.	.	.	8	.	.	.	8
Canada	.	.	.	.	.	.	.	7	.	7
South Korea	.	.	.	.	.	.	.	.	6	6
Tunisia	.	.	.	1	4	.	.	.	.	5
Peru	.	.	4	.	.	.	.	.	.	4
France	.	.	.	.	.	3	.	.	.	3
United States	.	.	.	.	.	2	.	.	.	2
Egypt	.	.	1	.	.	.	.	.	.	1
Germany	.	.	.	.	.	1	.	.	.	1
Spain	.	.	1	.	.	.	.	.	.	1
Sweden	.	.	.	.	.	.	.	1	.	1
Turkiye	.	.	.	.	1	.	.	.	.	1
Total	153					285				438

Table S9. Publications used for calibrating MP size distribution from various input sources.

Input sources	Publication
Organic fertilizers	
Organic fertilizers from large commercial producers across China, made from livestock manure, crop straws and other residues.	Zhao et al. 2023[8]
Organic fertilizers from local markets in Bangladesh.	Rana et al. 2023[9]
Organic fertilizers from local markets across China, made from livestock manures or bacterial residues.	Zhang et al. 2022[10]
Sludge from a wastewater treatment plant in Turkey.	Üstün et al. 2022[11]
Compostable organic fractions of municipal solid waste in Iran.	Fard et al. 2025[12]
Stabilized biosolids from water resource recovered facilities in United States and Canada.	Hazma et al. 2026[13]
Organic fertilizers from local markets in Hangzhou, China, made of manures, organic wastes or botanical ashes.	Qiu et al. 2026[14]
Wastewater irrigation	
Recycled irrigation water in Fuerteventura, Spain.	P.-R. et al. 2024[15]
Irrigation water system polluted by industrial and domestic waste-water in Taiwan, China.	Jiang et al. 2023[16]
Effluent water from a wastewater treatment plant in Israel.	Ben-David et al. 2021[17]
Effluent water from a wastewater treatment plant in Türkiye.	Üstün et al. 2022[11]
Atmospheric deposition	
Suburban and rural areas in Düzce, Türkiye.	Ertürk Arı et al. 2025[18]
The Alar agricultural zones in Xinjiang, China.	Du et al. 2024[19]
Rural and natural areas around the Thulamela, South Africa.	Mutshekwa et al. 2025[20]
Urbanized coastal zones of Gdynia, Poland.	Szewc et al. 2021[21]
Rural and suburban areas of Chengdu, central-west China.	Chen et al. 2024[22]
A wetland park in Guilin, southwestern China.	Zhang et al. 2025[23]
Rural areas of Wenzhou, eastern China.	Liao et al. 2021[24]
Low-population-density areas in Wuhan, China.	Zhu et al. 2024[25]
Suburban area in Champs-sur-Marne, northern France.	Beaurepaire et al. 2024[26]
Rural regions in North China Plain.	Li et al. 2023[27]
Suburb area of Hamburg, northern Germany.	Klein & Fischer 2019[28]
Farmlands in Beijing, China.	Lu et al. 2024[29]
Rural sites across Tuscany, central Italy.	Jafarova et al. 2025[30]

Table S10. Parameter names, corresponding variables in the model structure, and their search spaces in the optimization process.

Parameter	Variable	$\log_{10} X$	Min	Max
`a0`	a_0 in equation (4)	Yes	10^{-20}	10^{0}
`a1`	a_1 in equation (4)	Yes	10^{-20}	10^{0}
`delta_a`	δ_a in equation (4)	Yes	10^{-20}	10^{0}
`b0`	b_0 in equation (4)	Yes	10^{-20}	10^{0}
`b1`	b_1 in equation (4)	Yes	10^{-20}	10^{0}
`theta`	θ in equation (3)	No	0	9
`beta`	β in equation (3)	No	0.1	10
`macro_1`	Mulching input* in equation (5)	No	0	5
`macro_2`	Greenhouse input* in equation (5)	No	0	5
`macro_3`	Littering input* in equation (5)	No	0	5
`micro_1`	Organic fertilizer input* in equation (5)	No	0	5
`micro_2`	Wastewater irrigation input* in equation (5)	No	0	5

* Total mass of the input array, in units of parent particle mass ($k = 0$).

Table S11. Primary Köppen climate types and UV irradiation levels of provincial-level regions in China. The table only includes provincial-level regions whose data is available from the China Rural Statistical Yearbooks. For regions with multiple climate types, we mainly focus on the climate types of agricultural areas.

Climate	UV level	Provincial-level regions
Am/Aw	High	Hainan
Bs/Bw	High	Shanxi, Inner Mongolia, Shaanxi, Gansu, Ningxia, Xinjiang
ET	High	Tibet, Qinghai
Cf/Cw	Low	Shanghai, Jiangsu, Zhejiang, Anhui, Fujian, Jiangxi, Hubei, Hunan, Chongqing, Sichuan, Guizhou, Henan, Guangdong, Guangxi, Yunnan
Dw	Low	Beijing, Tianjin, Hebei, Liaoning, Jilin, Heilongjiang, Shandong

Supplementary Figures

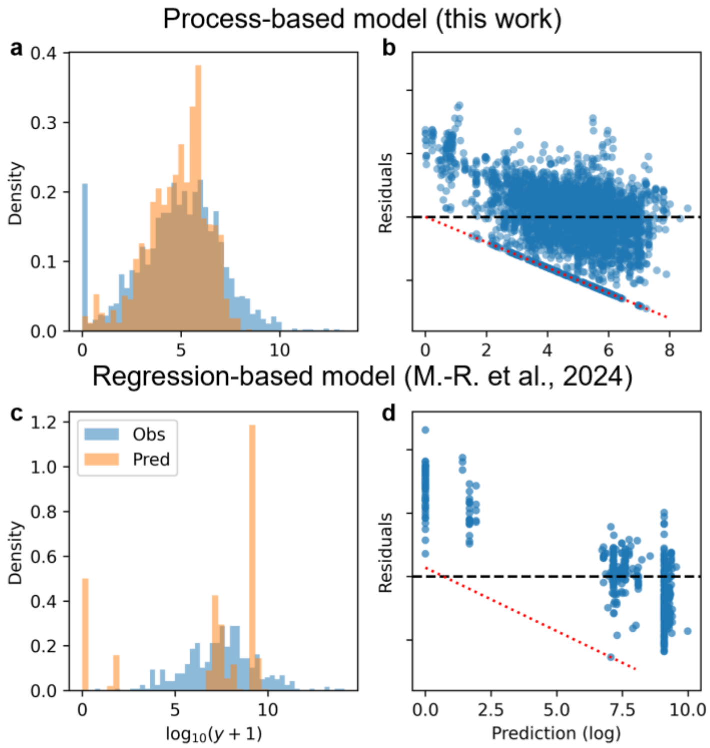

Figure S1. Distribution of predicted values, observations, and residuals after logarithmic transformation. Panel **(a)–(b)** are the results of the median values of prediction from the process-based model of this work, while panel **(c)–(d)** are the results of a regression-based model adapted from Meizoso-Regueira et al.[7] The blue histograms in **(a)** and **(c)** represent the distributions of observational data, and the orange histograms show the distributions of model predictions. Blue scatters in panel **(b)** and **(d)** mark the residuals for each data point, the black horizontal lines denote the zero baseline, and red dotted lines represent the diagonal boundary which is a mathematical artifactual for non-negative data in the log space.

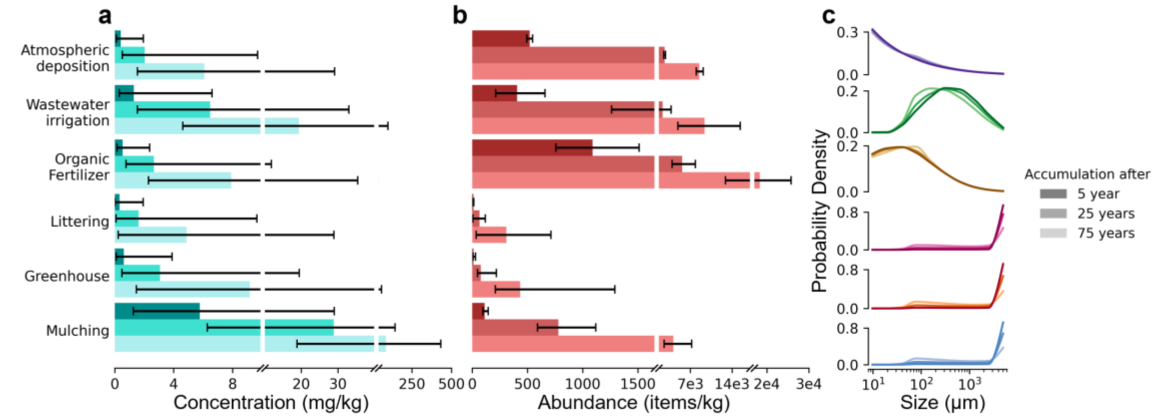

Figure S2. Simulated MP accumulation in annual crop sites under low UV climates after 5, 25 and 75 years of different continuous inputs. (a) MP mass concentrations (mg/kg) for different sources (atmospheric deposition, wastewater irrigation, organic fertilizer application, unmanaged littering, plastic greenhouses and mulch films). **(b)** Corresponding particle abundances (items/kg). Bars denote median values and error bars indicate the interquartile range (Q1–Q3) derived from bootstrap simulations. **(c)** The evolution of size distributions (probability density functions, PDF) for each source, shown as the median values of model simulation.

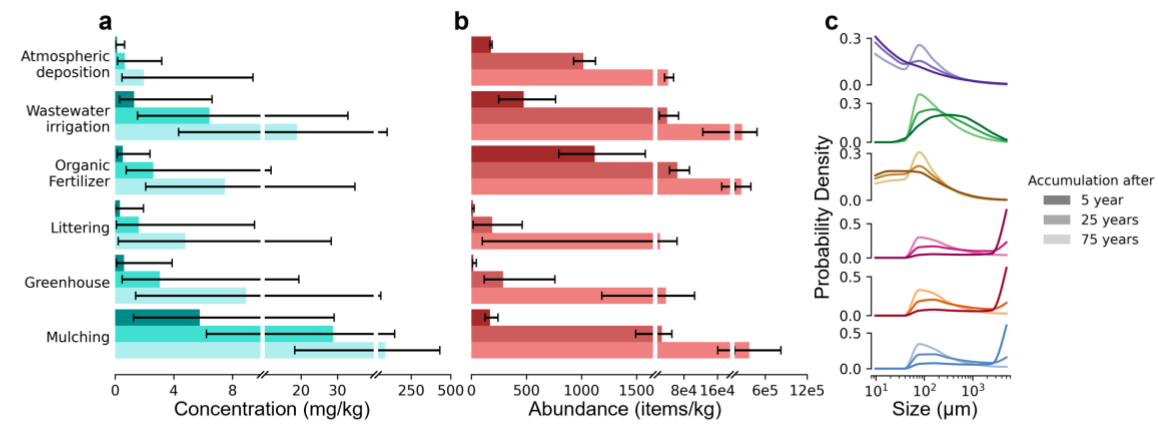

Figure S3. Simulated MP accumulation in perennial crop sites under high UV climates after 5, 25 and 75 years of different continuous inputs. (a) MP mass concentrations (mg/kg) for different sources (atmospheric deposition, wastewater irrigation, organic fertilizer application, unmanaged littering, plastic greenhouses and mulch films). **(b)** Corresponding particle abundances (items/kg). Bars denote median values and error bars indicate the interquartile range (Q1–Q3) derived from bootstrap simulations. **(c)** The evolution of size distributions (probability density functions, PDF) for each source, shown as the median values of model simulation.

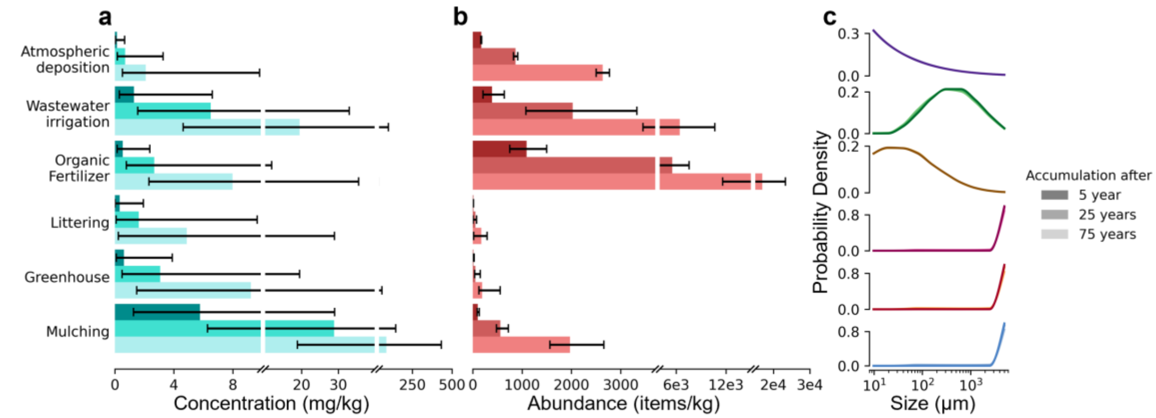

Figure S4. Simulated MP accumulation in perennial crop sites under low UV climates after 5, 25 and 75 years of different continuous inputs. (a) MP mass concentrations (mg/kg) for different sources (atmospheric deposition, wastewater irrigation, organic fertilizer application, unmanaged littering, plastic greenhouses and mulch films). **(b)** Corresponding particle abundances (items/kg). Bars denote median values and error bars indicate the interquartile range (Q1–Q3) derived from bootstrap simulations. **(c)** The evolution of size distributions (probability density functions, PDF) for each source, shown as the median values of model simulation.

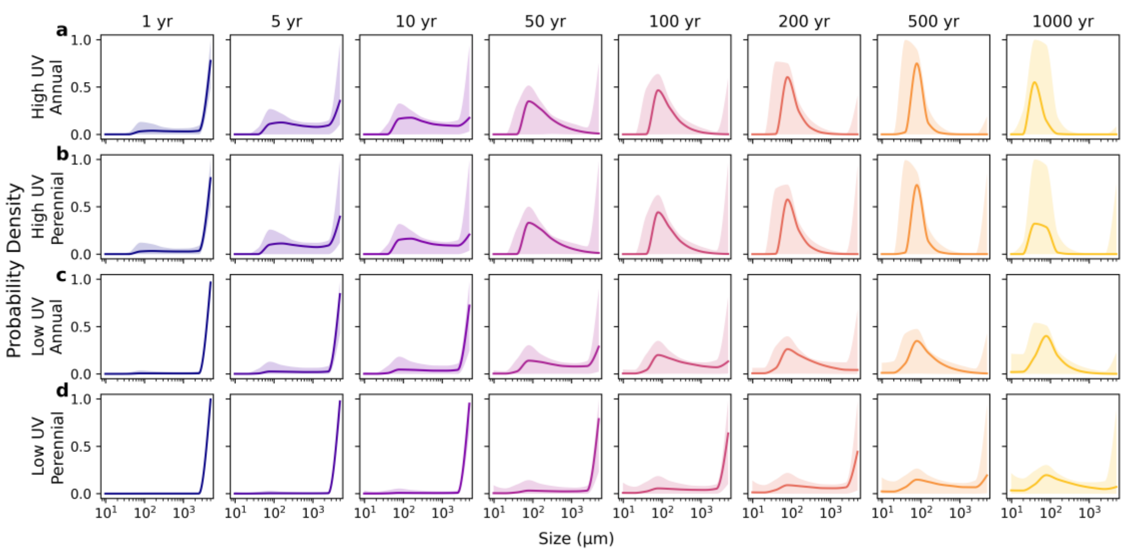

Figure S5. Simulated theoretical evolution of MP size distributions for a single parent particle input under (a) high-UV with annual cropping, (b) high-UV with perennial cropping, (c) low-UV with annual cropping, and (d) low-UV with perennial cropping. Curves represent the median relative abundance across size classes after 1, 5, 10, 50, 100, 200, 500, and 1000 years, and shaded bands indicate the 5–95% uncertainty.

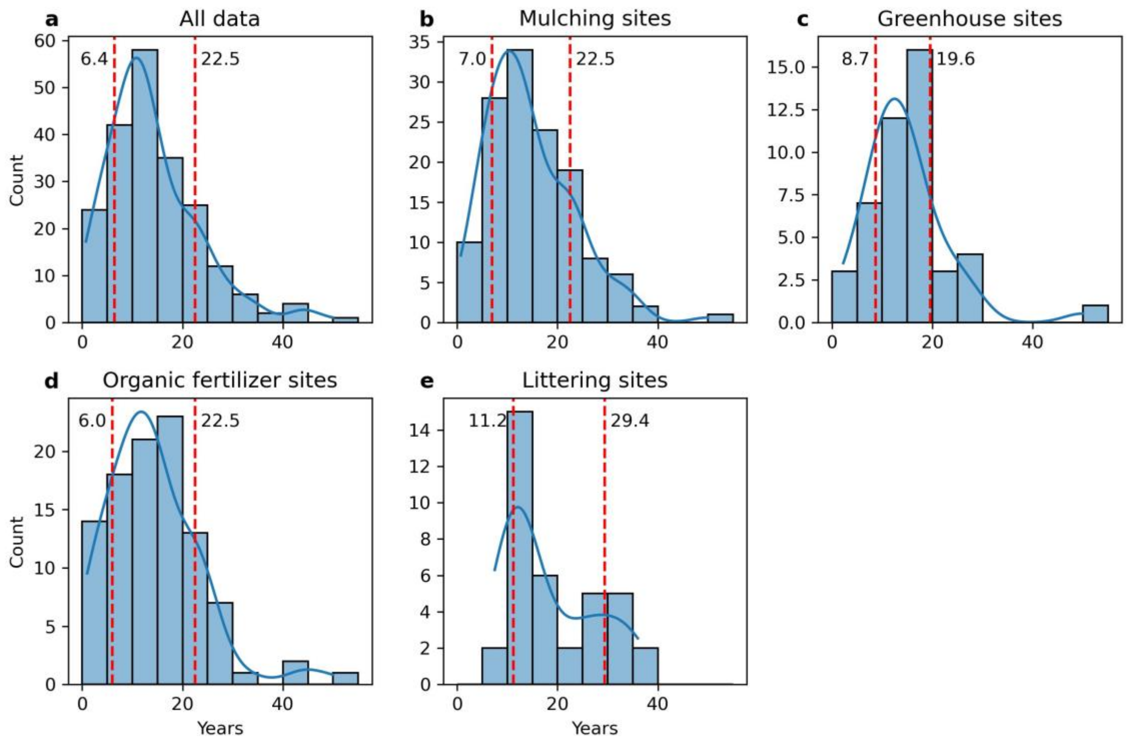

Figure S6. Distribution of site planting history on (a) all sites with available planting history information, and subsets with **(b)** mulching, **(c)** greenhouses, **(d)** organic fertilizers, and **(e)** littering. Solid lines show the kernel density curves, and vertical dashed lines denotes the range of the 60% central quantile intervals (20–80%).

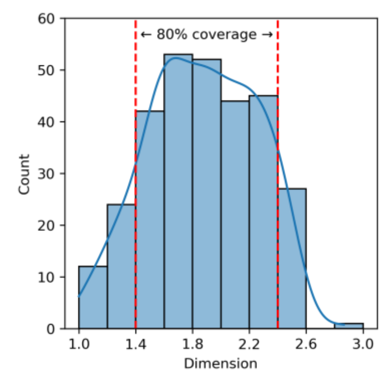

Figure S7. Histogram of MP particle dimensions (D_N) from literature data. Solid lines show the kernel density curves, and vertical dashed lines denotes the range of D_N in the fragmentation model (1.4–2.4), which covers around 80% of the distribution.

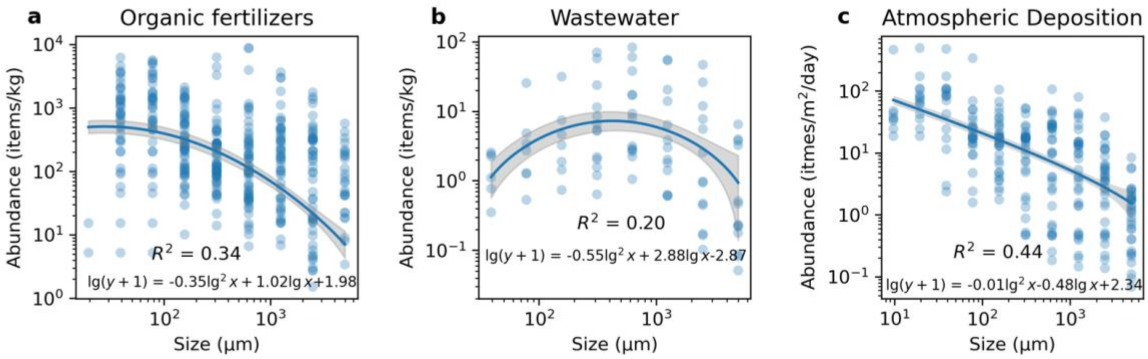

Figure S8. Size distributions of MP from different input sources: (a) organic fertilizers, **(b)** wastewater, and **(c)** atmospheric deposition. Literature-derived MP abundance data for each size bin are shown as scatter points. These data were then log-transformed and modeled using quadratic regression. Solid lines are the fitted regression curve, and grey bands indicate the 95% confidence intervals for the fits.

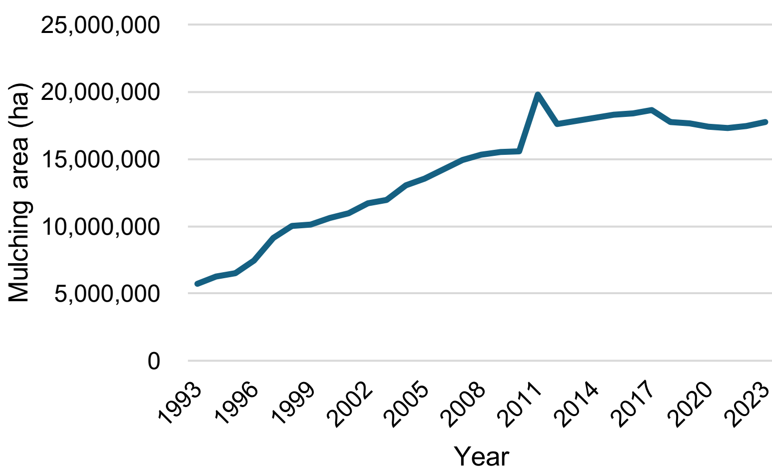

Figure S9. Annual total area of plastic mulching (hectares) in China. Data acquired from the *China Rural Statistical Yearbook.*[31] The nationwide mulching area increased for more than three times from 1993 to 2023.

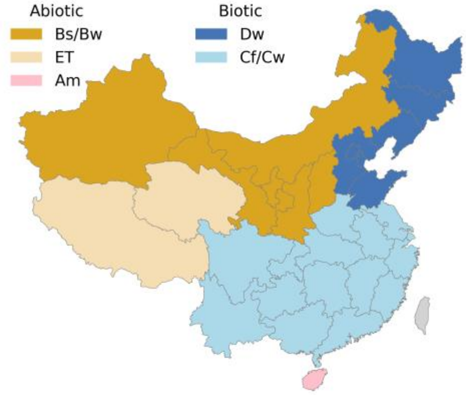

Figure S10. Provincial-level classification of primary Köppen climate types. Color coding: dark yellow – Bs or Bw; light yellow – ET; pink – Am; dark blue – Dw; light blue – Cf or Cw; grey – no data.

References

1. Kaandorp, M. L. A., Dijkstra, H. A. & Van Sebille, E. Modelling size distributions of marine plastics under the influence of continuous cascading fragmentation. *Environ. Res. Lett.* **16**, 054075 (2021).
2. Zhao, Z. *et al.* Irrigation-facilitated low-density polyethylene microplastic vertical transport along soil profile: An empirical model developed by column experiment. *Ecotoxicol. Environ. Saf.* **247**, 114232 (2022).
3. Park, S., Kim, I., Jeon, W.-H. & Moon, H. S. Exploring the vertical transport of microplastics in subsurface environments: Lab-scale experiments and field evidence. *J. Contam. Hydrol.* **257**, 104215 (2023).
4. Schefer, R. B., Koestel, J. & Mitrano, D. M. Minimal vertical transport of microplastics in soil over two years with little impact of plastics on soil macropore networks. *Commun. Earth Environ.* **6**, 278 (2025).
5. Chamas, A. *et al.* Degradation Rates of Plastics in the Environment. *ACS Sustain. Chem. Eng.* **8**, 3494–3511 (2020).
6. Liao, J. & Chen, Q. Biodegradable plastics in the air and soil environment: Low degradation rate and high microplastics formation. *J. Hazard. Mater.* **418**, 126329 (2021).
7. Meizoso-Regueira, T., Fuentes, J., Cusworth, S. J. & Rillig, M. C. Prediction of future microplastic accumulation in agricultural soils. *Environ. Pollut.* **359**, 124587 (2024).
8. Zhao, H. *et al.* Microplastic pollution in organic farming development cannot be ignored in China: Perspective of commercial organic fertilizer. *J. Hazard. Mater.* **460**, 132478 (2023).
9. Rana, Md. M., Haque, Md. R., Tasnim, S. S. & Rahman, Md. M. The potential contribution of microplastic pollution by organic fertilizers in agricultural soils of Bangladesh: quantification, characterization, and risk appraisals. *Front. Environ. Sci.* **11**, 1205603 (2023).
10. Zhang, S. *et al.* Occurrence and distribution of microplastics in organic fertilizers in China. *Sci. Total Environ.* **844**, 157061 (2022).
11. Üstün, G. E., Bozdaş, K. & Can, T. Abundance and characteristics of microplastics in an urban wastewater treatment plant in Turkey. *Environ. Pollut.* **310**, 119890 (2022).
12. Panahi Fard, M. *et al.* Microplastics in MSW-derived compost: release rate, characteristics, ecological risks, and mitigation strategies for sustainable agriculture. *Environ. Pollut. Bioavailab.* **37**, 2529998 (2025).
13. Hamza, M. *et al.* Variation in microplastic characteristics during biosolid stabilization across wastewater resource recovery facilities in the United States and Canada. *J. Environ. Manage.* **397**, 128374 (2026).
14. Qiu, Q. *et al.* An Evaluation of Potential Microplastic Risk from Commercial Organic Fertilizers. *Waste Biomass Valorization* **17**, 247–256 (2026).
15. Pérez-Reverón, R. *et al.* Recycled wastewater as a potential source of microplastics in irrigated soils from an arid-insular territory (Fuerteventura, Spain). *Sci. Total Environ.* **817**, 152830 (2022).
16. Jiang, J.-J. *et al.* Current levels and composition profiles of microplastics in irrigation water. *Environ. Pollut.* **318**, 120858 (2023).
17. Ben-David, E. A. *et al.* Microplastic distributions in a domestic wastewater treatment plant: Removal efficiency, seasonal variation and influence of sampling technique. *Sci. Total Environ.* **752**, 141880 (2021).
18. Ertürk Arı, P. *et al.* Atmospheric microplastic dispersion in diverse land-use context: insight from the black sea coastal region in Türkiye. *Air Qual. Atmos. Health* **18**, 1729–1743 (2025).

19. Du, A. *et al.* Distribution Characteristics of Atmospheric Microplastics in Typical Desert Agricultural Regions. *Environ. Toxicol. Chem.* **43**, 1982–1995 (2024).
20. Mutshekwa, T. *et al.* Atmospheric deposition of microplastics in urban, rural, forest environments: A case study of Thulamela Local Municipality. *PLOS ONE* **20**, e0313840 (2025).
21. Szewc, K., Graca, B. & Dołęga, A. Atmospheric deposition of microplastics in the coastal zone: Characteristics and relationship with meteorological factors. *Sci. Total Environ.* **761**, 143272 (2021).
22. Chen, Y. *et al.* Quantification and Characterization of Fine Plastic Particles as Considerable Components in Atmospheric Fine Particles. *Environ. Sci. Technol.* **58**, 4691–4703 (2024).
23. Zhang, L. *et al.* Atmospheric microplastic deposition in Guilin karst wetlands: Sources and agricultural impact. *Atmos. Pollut. Res.* **16**, 102537 (2025).
24. Liao, Z. *et al.* Airborne microplastics in indoor and outdoor environments of a coastal city in Eastern China. *J. Hazard. Mater.* **417**, 126007 (2021).
25. Zhu, J. *et al.* Atmospheric deposition is an important pathway for inputting microplastics: Insight into the spatiotemporal distribution and deposition flux in a mega city. *Environ. Pollut.* **341**, 123012 (2024).
26. Beaurepaire, M., Gasperi, J., Tassin, B. & Dris, R. COVID lockdown significantly impacted microplastic bulk atmospheric deposition rates. *Environ. Pollut.* **344**, 123354 (2024).
27. Li, J. *et al.* Atmospheric deposition of microplastics in a rural region of North China Plain. *Sci. Total Environ.* **877**, 162947 (2023).
28. Klein, M. & Fischer, E. K. Microplastic abundance in atmospheric deposition within the Metropolitan area of Hamburg, Germany. *Sci. Total Environ.* **685**, 96–103 (2019).
29. Lu, L. *et al.* Occurrence, influencing factors and sources of atmospheric microplastics in peri-urban farmland ecosystems of Beijing, China. *Sci. Total Environ.* **912**, 168834 (2024).
30. Jafarova, M., Aherne, J. & Loppi, S. Regional sources drive atmospheric microplastic deposition at rural background sites. *Environ. Res.* **285**, 122663 (2025).
31. Department of Rural Socioeconomic Survey. China rural statistical yearbook. China Statistics Press (2024).